The IMD and JNK pathways drive the functional integration of the immune and circulatory systems of mosquitoes

Yan Yan [1#], Leah T. Sigle [1#], David C. Rinker [1], Tania Y. Estévez-Lao [1], John A. Capra [1,2] and Julián F. Hillyer [1*]

[1] Department of Biological Sciences, Vanderbilt University, Nashville, TN, USA

[2] Bakar Computational Health Sciences Institute and Department of Epidemiology and Biostatistics, University of California San Francisco. San Francisco, CA, USA

[#] Contributed equally

* Corresponding author: julian.hillyer@vanderbilt.edu

Author contributions: Designed the research: YY, LTS, JFH; Performed the research: YY, LTS, TYE; Contributed new reagents/analytical tools: JAC, JFH; Analyzed data: YY, LTS, DCR, JFH; Wrote the paper: YY, JFH

Keywords: Hemocytes; Heart; Insect; Melanization; Phagocytosis

Abstract

The immune and circulatory systems of animals are functionally integrated. In mammals, the spleen and lymph nodes filter and destroy microbes circulating in the blood and lymph, respectively. In insects, immune cells that surround the heart valves (ostia), called periostial hemocytes, destroy pathogens in the areas of the body that experience the swiftest hemolymph (blood) flow. An infection recruits additional periostial hemocytes, amplifying heart-associated immune responses. Although the structural mechanics of periostial hemocyte aggregation have been defined, the genetic factors that regulate this process remain less understood. Here, we conducted RNAseq in the African malaria mosquito, *Anopheles gambiae*, and discovered that an infection upregulates multiple components of the IMD and JNK pathways in the heart with periostial hemocytes. This upregulation is greater in the heart with periostial hemocytes than in the circulating hemocytes or the entire abdomen. RNAi-based knockdown then showed that the IMD and JNK pathways drive periostial hemocyte aggregation and alter phagocytosis and melanization on the heart, thereby demonstrating how these pathways regulate the functional integration between the immune and circulatory systems. Understanding how insects fight infection lays the foundation for novel strategies that could protect beneficial insects and harm detrimental ones.

39 **Introduction**

40 Insect immune cells, called hemocytes, produce pattern recognition receptors
41 that detect microbial invaders, activate immune signaling pathways, and kill pathogens
42 via phagocytosis, lysis, melanization and other mechanisms (Hillyer, 2016; Hillyer &
43 Strand, 2014; Strand, 2008). These hemocytes exist in a dynamic body cavity called the
44 hemocoel, where the flow of hemolymph constantly circulates them throughout the
45 body. However, not all hemocytes circulate; one quarter of hemocytes are attached to
46 tissues and remain sessile (King & Hillyer, 2013). A sub-population of these sessile
47 hemocytes concentrates on the outer surface of the heart and, more specifically, in the
48 regions surrounding heart valves called ostia (King & Hillyer, 2012; Sigle & Hillyer,
49 2016). These heart-associated hemocytes, called periostial hemocytes, reside in the
50 locations of the body that experience the highest hemolymph flow, and intensely
51 phagocytose bacteria and malaria parasites within seconds of their entry into the
52 hemocoel. As this is happening, additional hemocytes leave circulation and aggregate
53 in the periostial regions of the heart, thereby augmenting the heart-associated immune
54 response (King & Hillyer, 2012; Sigle & Hillyer, 2016). Although the kinetics and
55 structural mechanics of periostial immunity have only been described in the African
56 malaria mosquito, *Anopheles gambiae* (King & Hillyer, 2012; League & Hillyer, 2016;
57 Sigle & Hillyer, 2016, 2018b, 2018c), the functional integration between the immune and
58 circulatory systems is conserved across the entire insect lineage (Yan & Hillyer, 2020).

59 In mosquitoes, pattern recognition receptors in the thioester-containing protein
60 family, together with adhesion and phagocytosis factors in the Nimrod protein family,
61 positively regulate immune responses on the heart (Sigle & Hillyer, 2018a; Yan &

62 Hillyer, 2019). However, heart-associated immune responses are triggered by both
63 bacterial and malarial infections, and by both peptidoglycan and B-1,3-glucan (King &
64 Hillyer, 2012; Sigle & Hillyer, 2016). Hence, the regulatory networks that drive periostial
65 hemocyte aggregation undoubtedly extend beyond pattern recognition receptors and
66 adhesion molecules. In insects, immune responses are primarily driven by pathways
67 such as Toll, immune deficiency (IMD), c-Jun N-terminal kinase (JNK), and Jak/Stat
68 (Hillyer, 2016). The Toll pathway acts via the transcription factor Rel1, and primarily
69 responds to Gram(+) bacteria, fungi and rodent malaria parasites, whereas the IMD and
70 interlinked JNK pathways act via the transcription factors Rel2 and JNK, respectively,
71 and primarily respond to Gram(–) bacteria and human malaria parasites (King, 2020;
72 Shaw & Catteruccia, 2019). In fruit flies, the Toll pathway is also involved in hemocyte
73 differentiation, and its constitutive activation disrupts sessile hemocytes (Banerjee,
74 Girard, Goins, & Spratford, 2019; Schmid et al., 2016). The IMD pathway has not been
75 directly linked to cellular immunity but its canonical activator, PGRP-LC, positively
76 regulates phagocytosis of *Escherichia coli* but not *Staphylococcus aureus* (Rämet,
77 Manfruelli, Pearson, Mathey-Prevot, & Ezekowitz, 2002). The Jak/Stat pathway acts via
78 the Stat family of transcription factors. In mosquitoes, this pathway responds to malaria
79 parasites and viruses (King, 2020; Shaw & Catteruccia, 2019), and in fruit flies it
80 controls hemocyte maturation and differentiation (Krzemień et al., 2007; Minakhina,
81 Tan, & Steward, 2011).

82 The goal of this study was to identify genes and regulatory pathways that drive
83 periostial hemocyte aggregation in *A. gambiae*. Using an unbiased RNA sequencing
84 (RNAseq) approach that was followed by empirical testing with RNA interference

85 (RNAi), we uncovered that the IMD and JNK pathways drive periostial hemocyte
86 aggregation and immune responses on the heart, thereby regulating the functional
87 integration between the immune and circulatory systems of mosquitoes.
88

89 **Results**

90 *Infection upregulates immune genes in periostial hemocytes*

91 To identify genes that may drive periostial hemocyte aggregation, we undertook
92 an unbiased RNAseq approach where we sequenced the transcriptome of tissues from
93 mosquitoes that were naïve, injured, or infected with Gram(–) GFP-*E. coli* or Gram(+) *S.*
94 *aureus* (Figure 1A-B; *Dataset* S1). Three tissues were isolated at 4 hr after treatment: (i)
95 the heart containing periostial hemocytes, (ii) the hemolymph containing circulating
96 hemocytes, and (iii) the entire abdomen. In these experiments, most mosquitoes were
97 used for sequencing, but a subset of mosquitoes was used to confirm that infection
98 induces heart-associated cellular immune responses. Indeed, a resident population of
99 periostial hemocytes was present in both naïve and injured mosquitoes, and the number
100 of periostial hemocytes increased 1.8- and 1.6-fold after GFP-*E. coli* and *S. aureus*
101 infection, respectively (Figure 1B-C).

102 RNAseq revealed that, relative to the heart and periostial hemocytes of naïve
103 and injured mosquitoes, 73 and 132 genes are upregulated more than 4-fold ($P < 0.05$)
104 in the heart and periostial hemocytes of mosquitoes infected with GFP-*E. coli* and *S.*
105 *aureus*, respectively (Figure 1D). Because periostial hemocyte aggregation is a dynamic
106 immune response that occurs during any bacterial infection, we hypothesized that its
107 core molecular drivers must be preferentially upregulated in periostial hemocytes

following both *E. coli* and *S. aureus* infection. We found that 55 genes met this overlap criterion (Figure 1E; Figure 1–figure supplement 1). Comparing the heart and periostial hemocyte RNAseq data to RNAseq data from (i) circulating hemocytes and (ii) the entire abdomen then revealed that infection upregulates more genes in the heart with periostial hemocytes than in the circulating hemocytes or the abdomen (Figure 1D-E; Figure 1–figure supplement 1-3).

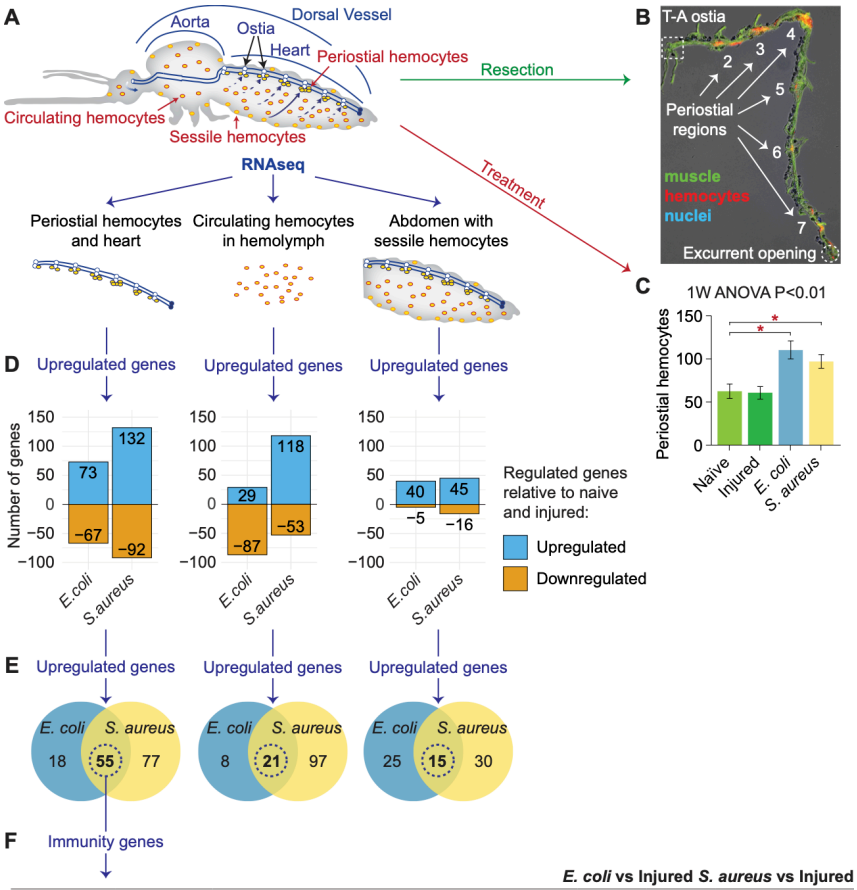

			E. coli vs Injured		*S. aureus* vs Injured	
Gene ID	**Gene name**	**Gene description**	**log2FC**	**P value**	**log2FC**	**P value**
AGAP000694	***cec3***	cecropin anti-microbial peptide	2.72	8E-14	3.20	2E-19
AGAP001212	*PGRPLB*	peptidoglycan recognition protein (long)	3.10	2E-25	4.21	3E-47
AGAP001648	*CLIPB17*	CLIP-domain serine protease	2.24	4E-10	3.01	3E-18
AGAP005205	***PGRPLA***	peptidoglycan recognition protein (long)	2.36	7E-47	2.66	1E-60
AGAP006747	***rel2***	NF-kappaB Relish-like transcription factor	2.00	2E-33	2.21	3E-41
AGAP009091	*ddc*	dopa decarboxylase	3.96	2E-50	4.81	3E-75
AGAP009213	*SRPN16*	serine protease inhibitor (serpin) 16	2.61	8E-13	3.75	1E-26
AGAP009214	*CLIPB11*	CLIP-domain serine protease	2.13	1E-06	3.71	2E-19
AGAP009460	***JNK3***	c-Jun N-terminal kinase	2.22	1E-04	3.47	1E-10
AGAP011294	***def1***	defensin anti-microbial peptide	2.13	2E-05	2.70	1E-08
AGAP011326	***IAP2***	inhibitor of apoptosis 2	3.21	2E-38	3.29	1E-40
AGAP013506	*upd3a*	JAK/STAT pathway cytokine unpaired 3 variant A	3.89	2E-12	4.05	8E-14

Figure 1. Infection upregulates immune genes in periostial hemocytes. (*A*) The heart with periostial hemocytes, the circulating hemocytes, and the abdomen of mosquitoes that were naïve, injured, or infected with GFP-*E. coli* or *S. aureus* were sequenced by RNAseq at 4 hr post-treatment. (*B*) Fluorescence and DIC overlay shows

119 that the periostial hemocytes (red) remain attached to a resected heart (green). Image
120 is modified from Sigle and Hillyer (Sigle & Hillyer, 2018b), and reproduced according to
121 Creative Commons Attribution License CC BY. (*C*) Naïve and injured mosquitoes have
122 resident periostial hemocytes, but infection for 4 hr with GFP-*E. coli* or *S. aureus*
123 induces the aggregation of additional hemocytes at the periostial regions. Whiskers
124 show the standard error of the mean (S.E.M.; n = 14 for all groups). (*D*) Bar plots show
125 the number of genes significantly upregulated or downregulated at 4 hr after GFP-*E. coli*
126 or *S. aureus* infection in the periostial hemocytes and heart (left), the circulating
127 hemocytes (middle), and the entire abdomen (right). (*E*) Venn diagrams show that 55,
128 21 and 15 genes are significantly upregulated in the periostial hemocytes, the
129 circulating hemocytes and the abdomen, respectively, during both GFP-*E. coli* and *S.*
130 *aureus* infections. (F) Table listing the immune genes that are among the 55 genes that
131 were upregulated in the heart with periostial hemocytes following both GFP-*E. coli* or *S.*
132 *aureus* infection. Genes that participate in the IMD/JNK pathway are in bold.
133

134 We then scrutinized the reported function of the 55 candidate genes. Twelve
135 have immune function (Figure 1F), and strikingly, 6 are part of IMD and JNK pathway:
136 *PGRP-LA* (Gendrin et al., 2017), *IAP2* (Myllymäki, Valanne, & Rämet, 2014), *rel2*
137 (Garver et al., 2012; Meister et al., 2005), *cec3* (Meister et al., 2005), *def1* (Garver,
138 Dong, & Dimopoulos, 2009; Luna et al., 2006), and *JNK3* (Boutros, Agaisse, &
139 Perrimon, 2002; Souvannaseng et al., 2018). Multiple aspects of the IMD/JNK pathway
140 are represented: upstream components such as *PGRP-LA* and *IAP2*, and downstream
141 elements from both branches of the pathway, with the classical IMD cascade
142 represented by *rel2*, *cec3* and *def1*, and the bifurcation into the JNK pathway
143 represented by *JNK3* (Myllymäki et al., 2014; Silverman et al., 2003; Zhuang et al.,
144 2006) (Figure 1–figure supplement 4). Relevant to this finding, activating the IMD
145 pathway induces the expression of *eater* (Wong et al., 2017), which positively regulates
146 hemocyte adhesion in fruit flies and periostial hemocyte aggregation in mosquitoes
147 (Bretscher et al., 2015; Sigle & Hillyer, 2018a). The IMD pathway also induces the
148 expression of *TEP1*, which is involved in phagocytosis and periostial hemocyte

149 aggregation (Yan & Hillyer, 2019). The JNK pathway is associated with cell adhesion
150 and phagocytosis by regulating the cytoskeleton (Boutros et al., 2002; Etchegaray et al.,
151 2012). The JNK pathway also induces the expression of *draper* (Weavers, Evans,
152 Martin, & Wood, 2016) and *TEP1* (Souvannaseng et al., 2018), which affect periostial
153 hemocyte aggregation in mosquitoes (Sigle & Hillyer, 2018a; Yan & Hillyer, 2019).
154 All six IMD and JNK pathway genes identified in our unbiased screen were more
155 highly upregulated in the heart and periostial hemocytes than in the other tissues
156 (Figure 1–figure supplement 5). The remaining six candidate genes with immune
157 function that were identified in our screen – *CLIPB17*, *DDC*, *SRPN16*, *CLIPB11*, *PGRP-*
158 *LB* and *upd3k* – do not participate in a common pathway. Therefore, based on the
159 RNAseq analyses we hypothesized that the main driver of periostial hemocyte
160 aggregation is the IMD/JNK pathway.
161
162 *The IMD pathway positively regulates periostial hemocyte aggregation*
163 To determine whether the IMD pathway regulates periostial hemocyte
164 aggregation, we synthesized double-stranded RNA (dsRNA) to target the IMD cascade
165 transcription factor, *rel2*, and its negative regulator, *caspar*, and achieved RNAi-based
166 silencing of 43% and 37%, respectively, compared to the ds*bla(Ap^R)* control mosquitoes
167 (Figure 2–figure supplements 1-2). Moreover, because *Tep1* is (i) activated by the Rel2
168 arm of the IMD pathway (Feng et al., 2021; Frolet, Thoma, Blandin, Hoffmann, &
169 Levashina, 2006) and (ii) a positive driver of periostial hemocyte aggregation (Yan &
170 Hillyer, 2019), we measured its mRNA abundance in *rel2* and *caspar* RNAi mosquitoes.
171 Silencing of *rel2* did not alter *TEP1* mRNA abundance but silencing of *caspar* increased

172 it. Because *cec3* and *def1* are also activated by Rel2 (Garver et al., 2009; Luna et al.,
173 2006; Meister et al., 2005), we measured their mRNA abundance in RNAi mosquitoes.
174 Silencing of *rel2* decreased *cec3* and *def1* mRNA abundance whereas silencing of
175 *caspar* increased them (Figure 2–figure supplement 1). Overall, these data are
176 consistent with the role that the Rel2 arm of the IMD pathway plays in regulating *TEP1*,
177 *cec3* and *def1* expression.

178 To assess whether the IMD pathway drives heart-associated immune responses,
179 we compared the number and activity of periostial hemocytes in *rel2* and *caspar* RNAi
180 mosquitoes, relative to ds*bla(Ap^R)* control mosquitoes (Figure 2). As expected, infection
181 for 4 hr induced the aggregation of hemocytes at the periostial regions of ds*bla(Ap^R)*
182 mosquitoes, and this aggregation remained in place at 24 hr. In uninfected mosquitoes,
183 knocking down *rel2* did not change the number of periostial hemocytes, but at 4 hr
184 following infection, knockdown of *rel2* decreased the number of periostial hemocytes by
185 18%, relative to ds*bla(Ap^R)* mosquitoes (Figure 2A-B). At 24 hr post-infection, the effect
186 of *rel2* RNAi on periostial hemocyte aggregation was diminished. When we instead
187 knocked down *caspar*, the number of periostial hemocytes increased by 39% in
188 uninfected mosquitoes, and infection for 4 and 24 hr increased the number of periostial
189 hemocytes by 30% and 19%, respectively, relative to similarly treated ds*bla(Ap^R)*
190 mosquitoes. This shows that *rel2* positively regulates periostial hemocyte aggregation
191 whereas *caspar* negatively regulates this process.

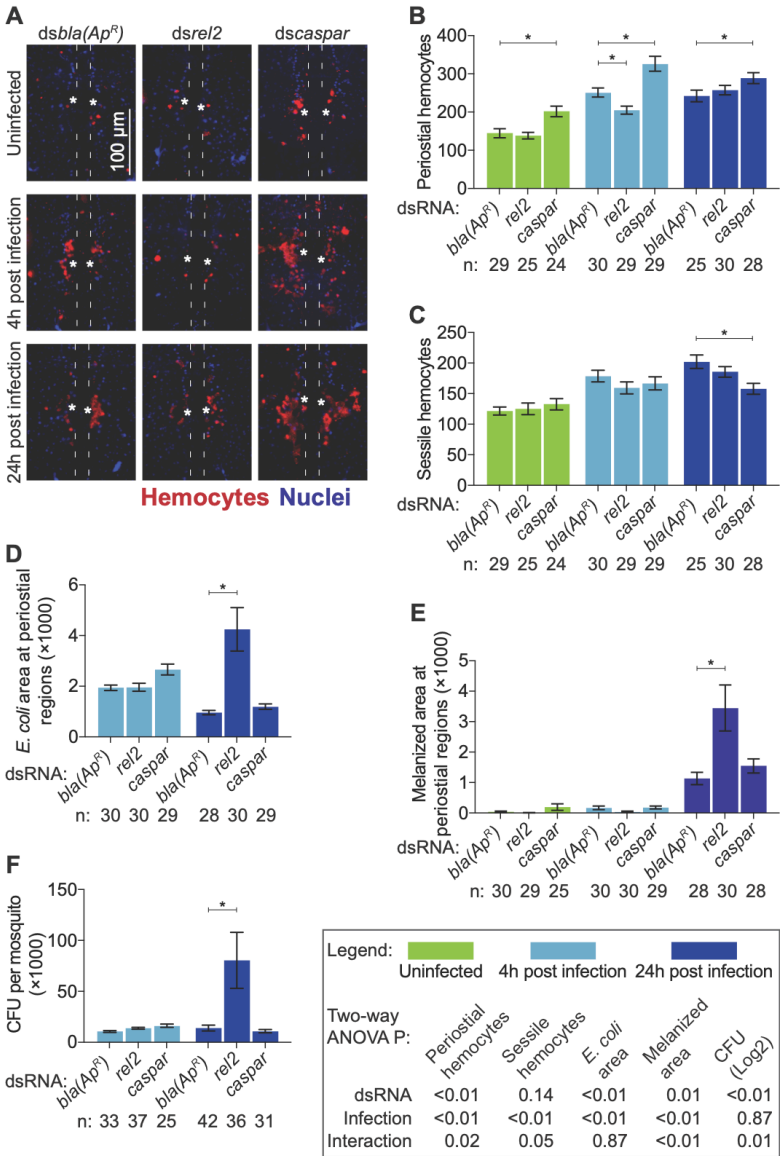

Figure 2. The IMD pathway drives periostial hemocyte aggregation. (*A*) Fluorescence images show periostial hemocytes (CM-DiI; red) surrounding a single pair of ostia (asterisks) on a segment of the heart (outlined by dotted lines) of ds*bla(Ap^R)*, ds*rel2* and ds*caspar* mosquitoes that were not infected or had been infected with GFP-*E. coli* for 4 or 24 hr. Anterior is on top. (*B-F*) Graphs for ds*bla(Ap^R)*, ds*rel2* and ds*caspar* mosquitoes that were not infected or had been infected with GFP-*E. coli* for 4 or 24 hr. The graphs show: (*B*) average number of periostial hemocytes; (*C*) average number of sessile hemocytes outside of the periostial regions in the tergum of abdominal segments 4 and 5; (*D*) pixel area of GFP-*E. coli* in the periostial regions; (*E*) pixel area of melanin in the periostial regions; and (*F*) the systemic GFP-*E. coli* infection intensity. Graphs in B-F show the mean and S.E.M. The data were analyzed by two-way ANOVA (bottom box), followed by Dunnett's multiple comparison test. N indicates sample size. Asterisks in graphs indicate post-hoc $P < 0.05$.

207 To determine whether the IMD pathway specifically affects periostial hemocytes
208 and not sessile hemocytes in general, we counted the number of sessile hemocytes
209 outside of the periostial regions in the tergum of abdominal segments 4 and 5 in the
210 same mosquitoes examined for periostial hemocytes (Figure 2C). Knockdown of *rel2* or
211 *caspar* did not alter the number of non-periostial sessile hemocytes in uninfected
212 mosquitoes or mosquitoes infected for 4 hr. However, at 24 hr following infection,
213 *caspar* RNAi decreased non-periostial sessile hemocytes by 22%. These results
214 demonstrate that the IMD pathway regulates periostial hemocyte aggregation while
215 having a minimal effect on the rest of the sessile hemocytes.
216 Periostial hemocytes phagocytose bacteria, leading to their accumulation at the
217 periostial regions (King & Hillyer, 2012; Sigle & Hillyer, 2016). To determine whether the
218 IMD pathway affects the phagocytic activity of periostial hemocytes, we measured the
219 GFP-*E. coli* fluorescence pixel area in the periostial regions of infected mosquitoes
220 (Figure 2D; Figure 2–figure supplement 3). At 4 hr following infection, the GFP-*E. coli*
221 pixel area was similar regardless of dsRNA treatment. At 24 hr after infection, this area
222 decreased in ds*bla(Ap^R)* and ds*caspar* mosquitoes, indicating that periostial hemocytes
223 efficiently destroyed the pathogens. However, at 24 hr following infection, *rel2* RNAi
224 significantly increased GFP-*E. coli* accumulation at the periostial regions. Periostial
225 hemocytes also phagocytose melanized bacteria (King & Hillyer, 2012; Sigle & Hillyer,
226 2016). Therefore, we measured melanin accumulation in the periostial regions (Figure
227 2E; Figure 2–figure supplement 3). Melanin was absent in uninfected mosquitoes and
228 mosquitoes that were infected for 4 hr. However, at 24 hr following infection, *rel2* RNAi

229 increased melanin deposits at the periostial regions whereas *caspar* RNAi had no
230 effect.

231 The increased accumulation of GFP-*E. coli* and melanin in *rel2* RNAi mosquitoes
232 at 24 hr after infection could be due to either (i) enhanced phagocytosis by periostial
233 hemocytes, or (ii) higher bacterial proliferation in the hemocoel, which places increased
234 pressure on the phagocytosis response. To differentiate between these two scenarios,
235 we measured the systemic GFP-*E. coli* infection intensity and observed that, at 4 hr after
236 infection, the bacterial intensity was similar for all dsRNA treatments, but at 24 hr,
237 knockdown of *rel2* resulted in a higher infection intensity than treatment with ds*caspar* or
238 ds*bla(Ap^R)* (Figure 2F). This suggests that *rel2* is essential for proper bacterial killing in
239 the hemocoel, and therefore, knocking it down increases infection intensity in a manner
240 that leads to increased phagocytosis in the periostial regions. However, because silencing
241 *rel2* and *caspar* had opposite effects on periostial hemocyte aggregation at 4 hr, a time
242 when dsRNA treatment does not impact infection intensity, we conclude that the IMD
243 pathway is a positive regulator of periostial hemocyte aggregation.

244 PGRP-LC is the canonical activator of the IMD pathway (Hillyer, 2016), but
245 PRGP-LA (i) activates the IMD pathway in the midgut of mosquitoes and in the barrier
246 epithelia of fruit flies (Gendrin et al., 2017; Gendrin et al., 2013), (ii) is expressed in
247 *Drosophila* hemocytes (Werner et al., 2000), and (iii) is upregulated in the heart and
248 periostial hemocytes (Figure 1F). *PGRP-LA* has three splice forms. To knock it down,
249 we synthesized ds*PGRP-LA-RARB* to target the *RA* and *RB* splice forms, and ds*PGRP-*
250 *LA-RC* to target the *RC* splice form. Using these dsRNAs, we achieved RNAi-based
251 silencing that ranged from 56% to 77%, compared to the ds*bla(Ap^R)* control mosquitoes

252 (Figure 3–figure supplement 1). *PGRP-LA* knockdown with any dsRNA did not alter the
253 number of periostial hemocytes, the number of non-periostial sessile hemocytes,
254 melanin accumulation at the periostial regions, or systemic infection intensity (Figure 3).
255 However, knockdown of *PGRP-LA-RC* increased phagocytosis of GFP-*E. coli* in the
256 periostial regions, which suggests that the RC splice form is involved in the
257 phagocytosis response.

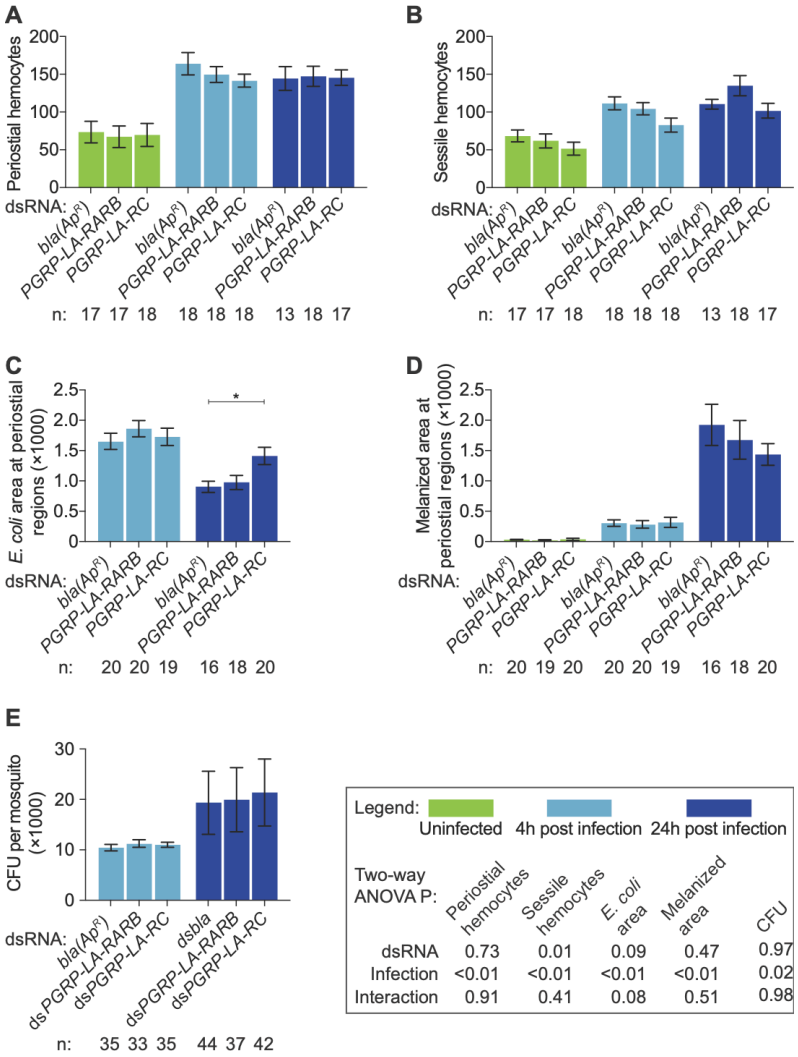

258
259 **Figure 3. The RC splice form of PGRP-LA regulates phagocytosis by periostial**
260 **hemocytes.** (*A-E*) Graphs for ds*bla(Ap^R)*, ds*PGRP-LA-RARB* and ds*PGRP-LA-RC*
261 mosquitoes that were not infected or had been infected with GFP-*E. coli* for 4 or 24 hr.
262 The graphs show: (*A*) average number of periostial hemocytes; (*B*) average number of
263 sessile hemocytes outside of the periostial regions in the tergum of abdominal
264 segments 4 and 5; (*C*) pixel area of GFP-*E. coli* in the periostial regions; (*D*) pixel area

265 of melanin in the periostial regions; and (*E*) the systemic GFP-*E. coli* infection intensity.
266 Graphs show the mean and S.E.M. The data were analyzed by two-way ANOVA
267 (bottom box), followed by Dunnett's multiple comparison test. N indicates sample size.
268 Asterisk in graph indicate post-hoc $p < 0.05$.
269

270 *The JNK pathway positively regulates periostial hemocyte aggregation*

271 We next tested whether the JNK pathway regulates periostial hemocyte
272 aggregation. *A. gambiae* encodes two JNK genes: *JNK1* and *JNK3* (Horton et al.,
273 2011). Therefore, we synthesized double-stranded RNA (dsRNA) to target the JNK
274 cascade transcription factors, *JNK1* and *JNK3*, and their negative regulator, *puckered*
275 (*puc*). Because of high sequence identity between *JNK1* and *JNK3*, ds*JNK1/3*
276 simultaneously targeted both JNK genes. RNAi-based knockdown resulted in 33%, 44%
277 and 31% reduction in mRNA abundance of *JNK1*, *JNK3* and *puc*, respectively (Figure
278 4–figure supplement 1). Moreover, because the JNK pathway has also been implicated
279 in the expression of *TEP1* (Garver, de Almeida Oliveira, & Barillas-Mury, 2013), we
280 measured the mRNA abundance of *TEP1*, *cec3* and *def1* in *JNK1*/*JNK3* and *puc* RNAi
281 mosquitoes. Manipulating the JNK pathway did not have a clear impact on effector gene
282 expression (Figure 4–figure supplement 1). The lack of clarity on how the JNK pathway
283 controls the expression of *TEP1*, *cec3* or *def1* is likely due to their co-regulation by other
284 pathways.

285 To assess whether the JNK pathway drives heart-associated immune responses,
286 we compared the number and activity of periostial hemocytes in *JNK1/3* and *puc* RNAi
287 mosquitoes, relative to ds*bla(Ap^R)* control mosquitoes (Figure 4). Regardless of
288 infection status, the number of periostial hemocytes was statistically similar between
289 ds*JNK1/3* and ds*bla(Ap^R)* mosquitoes, although ds*JNK1/3* mosquitoes averaged fewer

290 periostial hemocytes than control mosquitoes for all treatments (Figure 4A-B).
291 Knockdown of *puc*, however, increased the number of periostial hemocytes 1.6-fold in
292 uninfected mosquitoes, and 1.4- and 1.5-fold at 4 and 24 hr following GFP-*E. coli*
293 infection, respectively, relative to similarly treated ds*bla(Ap^R)* mosquitoes. To further
294 determine whether *puc* specifically affects periostial hemocytes or sessile hemocytes in
295 general, we quantified the number of non-periostial sessile hemocytes on the tergum of
296 the same mosquitoes (Figure 4C). *JNK1/3* RNAi mosquitoes showed a trend of fewer
297 non-periostial sessile hemocytes than control mosquitoes regardless of infection status.
298 Treatment with ds*puc*, however, increased the number of non-periostial sessile
299 hemocytes for all treatments. This demonstrates that the JNK pathway positively
300 regulates both periostial and non-periostial sessile hemocyte abundance.
301 We next measured whether the JNK pathway affects the phagocytic activity of
302 periostial hemocytes (Figure 4D; Figure 4–figure supplement 2). At 4 hr following
303 infection, the GFP-*E. coli* pixel area was similar regardless of dsRNA treatment.
304 However, at 24 hr following infection, periostial hemocytes in ds*puc* mosquitoes
305 phagocytosed more GFP-*E. coli* than the ds*bla(Ap^R)* mosquitoes. We then quantified
306 the melanized bacteria that were sequestered by periostial hemocytes (Figure 4E;
307 Figure 4–figure supplement 2). Melanin deposits were undetectable in uninfected
308 mosquitoes and mosquitoes at 4 hr post infection; however, at 24 hr following GFP-*E.*
309 *coli* infection, more melanin was present in ds*puc* mosquitoes than in ds*bla(Ap^R)*
310 controls.

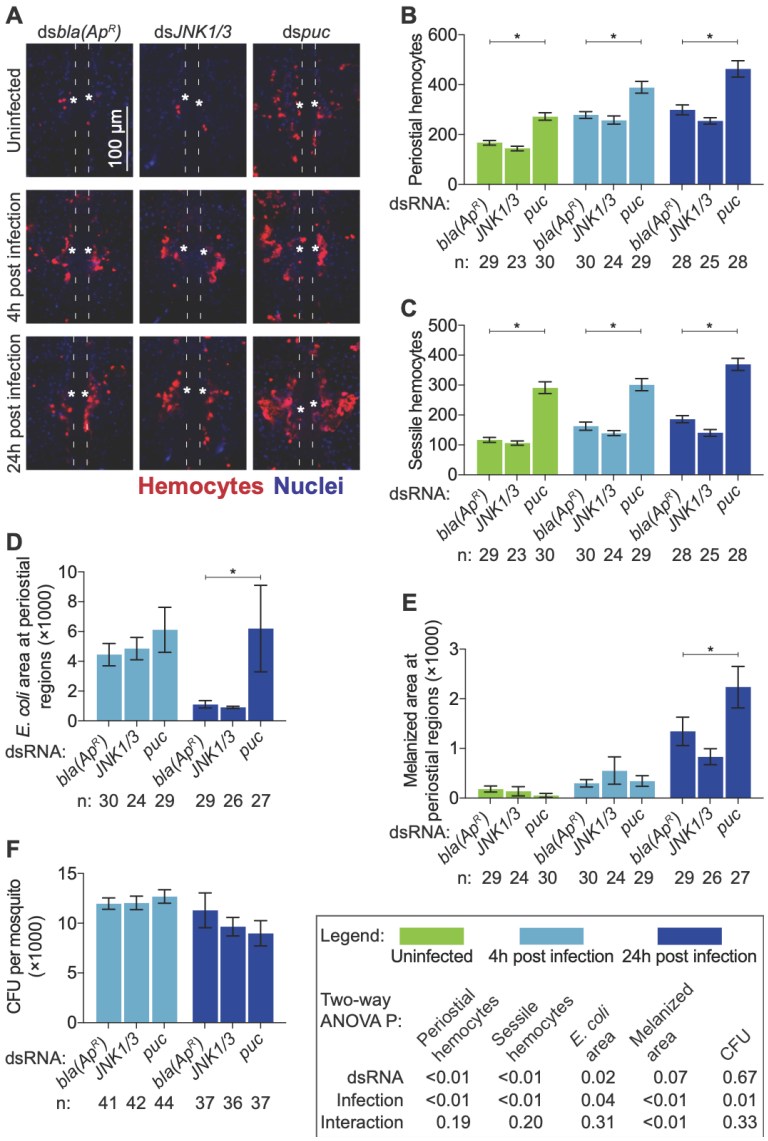

Figure 4. The JNK pathway drives periostial hemocyte aggregation. (*A*) Fluorescence images show periostial hemocytes (CM-DiI; red) surrounding a single pair of ostia (asterisks) on a segment of the heart (outlined by dotted lines) of ds*bla(Ap^R)*, ds*JNK1/3* and ds*puc* mosquitoes that were not infected or had been infected with GFP-*E. coli* for 4 or 24 hr. Anterior is on top. (*B-F*) Graphs for ds*bla(Ap^R)*, ds*JNK1/3* and ds*puc* mosquitoes that were not infected or had been infected with GFP-*E. coli* for 4 or 24 hr. The graphs show: (*B*) average number of periostial hemocytes; (*C*) average number of sessile hemocytes outside of the periostial regions in the tergum of abdominal segments 4 and 5; (*D*) pixel area of GFP-*E. coli* in the periostial regions; (*E*) pixel area of melanin in the periostial regions; and (*F*) the systemic GFP-*E. coli* infection intensity. Graphs in B-F show the mean and S.E.M. The data were analyzed by two-way ANOVA (bottom box), followed by Dunnett's multiple comparison test. N indicates sample size. Asterisks in graphs indicate post-hoc $P < 0.05$.

326 The difference in GFP-*E. coli* and melanin accumulation in ds*puc* mosquitoes
327 could be due to (i) enhanced phagocytosis by periostial hemocytes, or (ii) higher
328 bacterial proliferation in the hemocoel. To differentiate between these two scenarios, we
329 quantified the systemic *E. coli* infection intensity and found that the bacterial intensity
330 was similar regardless of dsRNA treatment (Figure 4F). Therefore, this suggests that
331 *puc* negatively regulates hemocyte adhesion and phagocytic activity, and demonstrates
332 that the JNK pathway is a positive regulator of periostial immune responses.
333

334 **Discussion**

335 Previous microarray and RNAseq analyses revealed genes and signaling
336 pathways that are active in hemocytes (Bartholomay et al., 2004; Baton, Robertson,
337 Warr, Strand, & Dimopoulos, 2009; Choi, Fuchs, Mayhew, Yu, & Christensen, 2012; H
338 Kwon & Smith, 2019; Pinto et al., 2009; Rani et al., 2021; Thomas et al., 2016),
339 including those that are activated in specific subpopulations of hemocytes (H. Kwon,
340 Mohammed, Franzén, Ankarklev, & Smith, 2021; Raddi et al., 2020; Severo et al.,
341 2018). However, these studies only focused on circulating hemocytes, and therefore,
342 failed to capture the biology of sessile hemocytes. Yet, one quarter of hemocytes are
343 sessile (King & Hillyer, 2013), and they play significant roles in hematopoiesis (Leitão &
344 Sucena, 2015; Márkus et al., 2009), wound healing (Babcock et al., 2008), and
345 pathogen killing (Horn, Leips, & Starz-Gaiano, 2014; Kocks et al., 2005; League &
346 Hillyer, 2016). Therefore, extrapolating the molecular signatures of circulating
347 hemocytes to those of sessile hemocytes likely misses the essential factors that make
348 sessile hemocytes conduct their specific immune activities. Periostial hemocytes are a

349 subpopulation of sessile hemocytes that reside on the heart, where they sequester and
350 kill pathogens in areas of high hemolymph flow (King & Hillyer, 2012; Sigle & Hillyer,
351 2016). To better understand how an infection drives the migration of hemocytes to the
352 heart and how these immune cells kill pathogens at the periostial regions, we
353 sequenced the periostial hemocyte transcriptome and discovered that the IMD/JNK
354 pathway drives periostial immune responses (Figure 5).

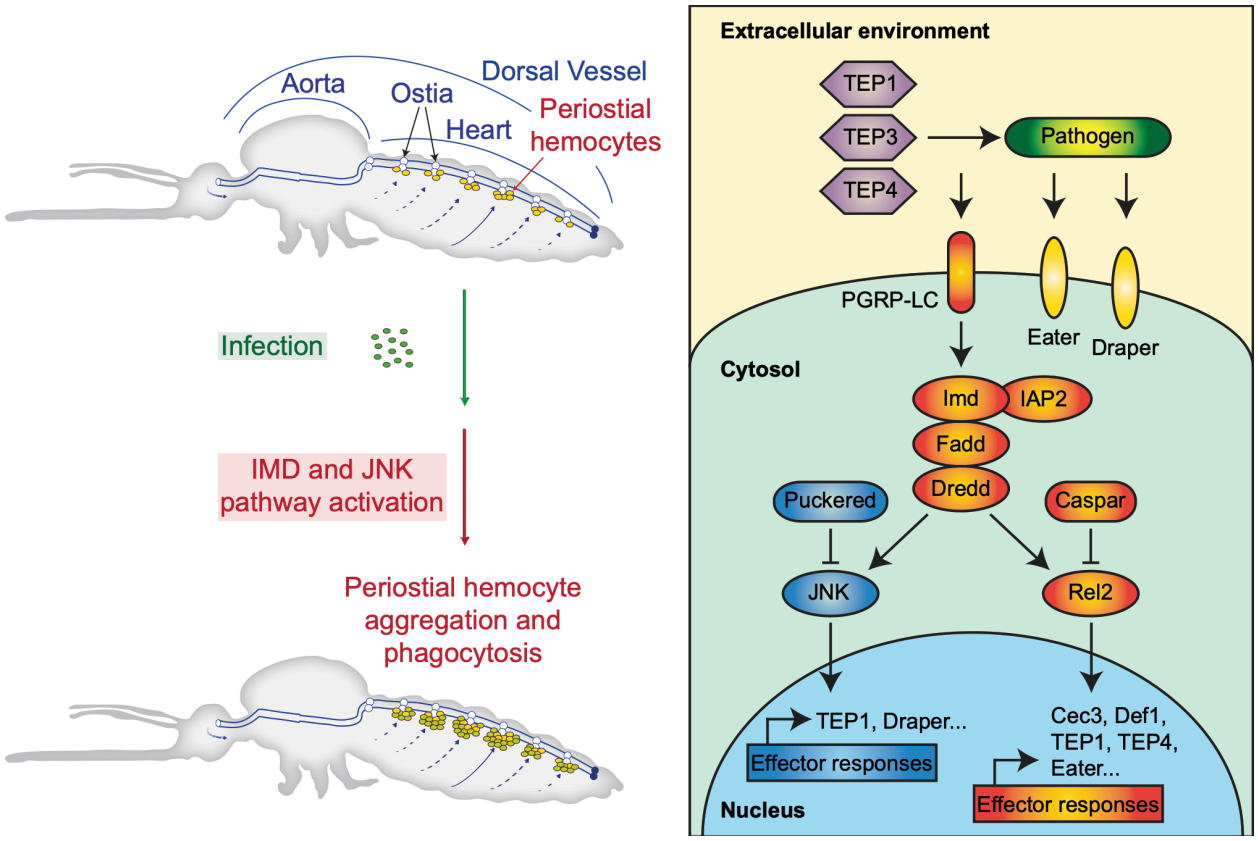

355
356
357 **Figure 5. The IMD and JNK pathways, together with TEP proteins (TEP1, TEP3**
358 **and TEP4) and Nimrod proteins (Draper and Eater), regulate heart-associated**
359 **immune responses in mosquitoes.**
360

361 The IMD pathway controls the production of antimicrobial peptides (Hillyer, 2016;
362 Myllymäki et al., 2014), but here we show that the IMD pathway also regulates a cellular
363 immune response: the transition of hemocytes from a circulating to a sessile state on

364 the heart. Specifically, knockdown of the positive regulator of the IMD pathway, *rel2*,
365 decreases infection-induced periostial hemocyte aggregation, whereas knockdown of
366 the negative regulator of the IMD pathway, *caspar*, increases the number of periostial
367 hemocytes. We hypothesize that the IMD pathway drives periostial hemocyte
368 aggregation via two cascades that are also driving phagocytosis: the TEP1-TEP3-
369 LRP1-CED6L and TEP4-BINT2-CED2L-CED5L pathways (Moita et al., 2005). The IMD
370 pathway induces the expression of *TEP1* and *TEP4* (Dong et al., 2011; Garver et al.,
371 2009; Luna et al., 2006), and both of these genes positively regulate periostial
372 hemocyte aggregation (Yan & Hillyer, 2019). Moreover, two downstream molecules –
373 LRP1 and BINT2 – are transmembrane proteins that in mammals and insects have
374 overlapping functions in phagocytosis and adhesion (Mantuano, Jo, Gonias, &
375 Campana, 2010; Moita, Vriend, Mahairaki, Louis, & Kafatos, 2006; Rabiej et al., 2016),
376 and therefore, likely facilitate the adhesion of hemocytes to the heart. In this study, we
377 also confirmed the positive role that REL2 plays in pathogen killing (Dekmak, Yang, Zu
378 Dohna, Buchon, & Osta, 2021; Dong et al., 2011; Dong, Simões, & Dimopoulos, 2020;
379 Frolet et al., 2006; Kambris et al., 2010; Khan, Liew, Leong, & Lau, 2016; Meister et al.,
380 2009; Meister et al., 2005; Mitri et al., 2009; Schnitger, Kafatos, & Osta, 2007). When
381 we systemically knocked down the expression of *rel2*, bacteria proliferated
382 uncontrollably during the later stages of infection. We hypothesize that knocking down
383 *rel2* initially suppresses periostial hemocyte aggregation, but as the infection progresses
384 and the intensity increases, the necessity of periostial immune responses also
385 increases, and this pressure recruits hemocytes to the heart and enhances their
386 collective phagocytic activity. Overall, our data show that the IMD pathway drives

387 periostial hemocyte aggregation during the early stages of infection and limits systemic
388 bacterial intensity during the later stages of infection.

389 The JNK pathway modulates mosquito longevity, regulates oviposition, and limits
390 infection with malaria parasites and viruses (Chowdhury et al., 2020; Garver et al.,
391 2013; Nsango et al., 2013; Peirce et al., 2020; Ramphul, Garver, Molina-Cruz, Canepa,
392 & Barillas-Mury, 2015; Souvannaseng et al., 2018). Here, we found that overexpressing
393 the JNK pathway by knocking down the negative regulator, *puc*, increases the number
394 of periostial and adjacent sessile hemocytes. This suggests that the JNK pathway
395 positively regulates hemocyte adhesion. Indeed, the *Drosophila* ortholog of mosquito
396 *JNK1* and *JNK3*, called *basket*, is involved in the formation of actin-rich and focal
397 adhesion kinase-rich placodes in hemocytes (Williams, Wiklund, Wikman, & Hultmark,
398 2006). The JNK pathway also induces hemocyte differentiation in *Drosophila*, producing
399 large lamellocytes that adhere and encapsulate parasitoid eggs (Zettervall et al., 2004).
400 We found that overactivating the JNK pathway does not alter infection intensity in
401 mosquitoes, but it increases the accumulation of *E. coli* and melanin on the heart,
402 suggesting that the JNK pathway positively regulates the phagocytosis and
403 melanization responses. Indeed, JNK1 positively regulates melanization in mosquitoes
404 that are refractory to malaria (Garver et al., 2013), and overexpressing the JNK pathway
405 in aphids increases the melanin-producing activity of phenoloxidase and the phagocytic
406 activity of hemocytes (Ma et al., 2020). We hypothesize that the JNK pathway regulates
407 phagocytosis by periostial hemocytes in a manner that involves two proteins already
408 known to be involved in periostial hemocyte aggregation: TEP1 and draper (Sigle &
409 Hillyer, 2018a; Yan & Hillyer, 2019). The JNK pathway activates the expression of both

410 of these genes (Macdonald, Doherty, Hackett, & Freeman, 2013; Peirce et al., 2020;
411 Souvannaseng et al., 2018), and TEP1 opsonizes pathogens for phagocytosis whereas
412 draper activates phagocytic processes (Evans, Rodrigues, Armitage, & Wood, 2015;
413 Levashina et al., 2001; Manaka et al., 2004; Moita et al., 2005; Sigle & Hillyer, 2018a;
414 Yan & Hillyer, 2019). In our study, we could not distinguish between the roles that *JNK1*
415 and *JNK3* play in periostial hemocyte aggregation. However, simultaneous knockdown
416 of both resulted in phenotypes that were opposite of *puc* knockdown, strongly
417 suggesting that JNK1 or JNK3 – or both – positively regulates periostial hemocyte
418 aggregation.

419 Because both the IMD and JNK pathways induce the production of *TEP1* (Dong
420 et al., 2011; Garver et al., 2009; Peirce et al., 2020; Souvannaseng et al., 2018), we
421 hypothesize that they share the TEP1-TEP3-LRP1-CED6L phagocytosis cascade that
422 leads to hemocyte aggregation. However, we also hypothesize that the IMD and JNK
423 pathways use additional, independent mechanisms to regulate periostial hemocyte
424 aggregation for three reasons. First, even though the two pathways share upstream
425 signaling molecules, they bifurcate and activate their own set of effector genes
426 (Silverman et al., 2003; Zhuang et al., 2006). Second, knocking down the components
427 of the IMD and JNK pathways resulted in different phenotypes, especially for periostial
428 and non-periostial sessile hemocytes. Third, in *Drosophila*, draper and the BINT2
429 ortholog (Integrin $\beta\nu$) function independently (Nagaosa et al., 2011), and in mosquitoes,
430 draper is regulated by the JNK pathway whereas BINT2 is involved in the IMD-regulated
431 and TEP4-mediated phagocytosis cascade (Luna et al., 2006; Macdonald et al., 2013;
432 Moita et al., 2006; Moita et al., 2005).

433 Bacteria, malaria parasites, and fungal components all induce periostial
434 hemocyte aggregation, and this process is structurally conserved across the entire
435 insect lineage (King & Hillyer, 2012; Sigle & Hillyer, 2016; Yan & Hillyer, 2020).
436 Therefore, it is likely that other proteins contribute to this process. Indeed, infection also
437 induces the upregulation of *Upd3* by periostial hemocytes, which is a ligand for the
438 receptor of the JAK/STAT pathway (Chakrabarti et al., 2016). The TOLL pathway also
439 induces hemocyte proliferation (Chiu et al., 2005; Qiu, Pan, & Govind, 1998) and the
440 expression of *TEP1* (Frolet et al., 2006), which positively regulates periostial hemocyte
441 aggregation (Yan & Hillyer, 2019). Beyond immune pathways, periostial hemocyte
442 aggregation may also be under the influence of neuronal and hormonal control. For
443 example, injecting mosquitoes with the neuropeptide, allatotropin, increases the number
444 of periostial and non-periostial sessile hemocytes (Hernández-Martínez et al., 2017).
445 Therefore, the regulation of periostial hemocyte aggregation is not expected to be
446 limited to the IMD and JNK pathways.
447 To date, we have tested the involvement of several hemocyte-produced factors
448 on periostial hemocyte aggregation. However, the heart itself may produce
449 complementary factors that drive this immune response. For example, a fibroblast
450 growth factor is highly regulated in the heart and periostial hemocytes. Its ortholog in
451 *Drosophila*, called *Branchless*, is expressed in the heart and pericardial cells, and
452 regulates hemocyte differentiation in the lymph glands of the larval heart (Destalminil-
453 Letourneau, Morin-Poulard, Tian, Vanzo, & Crozatier, 2021; Dragojlovic-Munther &
454 Martinez-Agosto, 2013). Moreover, reducing the expression of the *Drosophila* cardiac
455 extracellular matrix (ECM) proteins, *Pericardin* and *Laminin A*, disrupts the formation of

456 the cardiac ECM and lowers the number of hemocytes on the heart (Cevik, Acker,
457 Michalski, & Jacobs, 2019; Ghosh, Singh, Mandal, & Mandal, 2015). These data
458 suggest that the heart and its associated structures facilitate the binding of circulating
459 hemocytes to the periostial regions. Our RNAseq experiment also revealed that an
460 infection upregulates transglutaminases in the heart and periostial hemocytes, which
461 are known for crosslinking Rel2 and other proteins (Shibata et al., 2013), and thus, they
462 may also play a role in periostial hemocyte aggregation.

463 Heart-associated immune responses occur in insects from at least 16 different
464 taxonomic orders, including insects that are of agricultural, urban, and medical
465 importance (Yan & Hillyer, 2020). Understanding the genetic factors that drive periostial
466 hemocyte aggregation in *A. gambiae* sheds light on how this medically important insect
467 and other insects of societal importance fight the pathogens that invade them. Indeed,
468 the TEP gene family, the Nimrod gene family (Eater, Nimrod and Draper) and the JNK
469 pathway are conserved amongst insects (Blandin & Levashina, 2004; Bou Aoun et al.,
470 2011; Horton et al., 2011; Somogyi et al., 2008), and although some insects in the order
471 Hemiptera lack components of the IMD pathway, all insects queried to date still have a
472 functional IMD-based immune response (Gerardo et al., 2010; Mesquita et al., 2015;
473 Nishide et al., 2019; Salcedo-Porras, Guarneri, Oliveira, & Lowenberger, 2019).
474 Therefore, we conclude that the IMD and JNK pathways, together with TEP and Nimrod
475 proteins, are primary regulators of the heart-associated immune responses in insects.
476

477 **Materials and Methods**

478 *Mosquitoes, bacteria, infection, and replication*

479 *Anopheles gambiae,* Giles sensu stricto (G3; Diptera: Culicidae), were
480 maintained at 27 °C, 75% relative humidity, and a 12 hr:12 hr light:dark photoperiod
481 (Glenn, King, & Hillyer, 2010). Experiments were done using female adults fed 10%
482 sucrose. Tetracycline resistant, GFP-expressing *E. coli* (modified DH5α; GFP-*E. coli*)
483 and *S. aureus* (RN6390) were grown in Luria-Bertani (LB) and tryptic soy broth,
484 respectively, at 37 °C in a shaking incubator. Dilutions of the bacterial cultures were
485 injected at the thoracic anepisternal cleft using a Nanoject III (Drummond Scientific
486 Company, Broomall, PA). The infection dose was determined by plating the cultures
487 and counting the colony forming units (CFUs).
488 In this study, a biological replicate is an independent experiment that utilizes
489 mosquitoes from an independent egg batch. A technical replicate is an experimental
490 resampling of a biological replicate. All data collected were included in the analysis; no
491 data were excluded.
492
493 *RNAseq: treatment, tissue collection, RNA isolation and library preparation*
494 Six-day-old mosquitoes were randomly divided into four groups: (i) naïve
495 (unmanipulated), (ii) injured by injecting 69 nL of sterile LB, (iii) infected by injecting 69
496 nL of GFP-*E. coli* (~75,779 CFUs), and (iv) infected by injecting 69 nL of *S. aureus*
497 (~39,451 CFUs). Four hr after treatment, three tissues were isolated: (i) the heart with
498 periostial hemocytes, (ii) hemolymph with circulating hemocytes, and (iii) the entire
499 abdomen. To isolate the heart, mosquitoes were bisected along the coronal plane in
500 RNase-free PBS, and the heart with the periostial hemocytes was resected by severing
501 the alary muscles and detaching it from the cuticle (Sigle & Hillyer, 2018b). To isolate

502 circulating hemocytes, hemolymph was perfused by making an incision in the last
503 abdominal segment, injecting RNase-free PBS into the hemocoel through the cervical
504 membrane, and collecting the first 2 drops that exited the abdomen (Hillyer &
505 Christensen, 2002). The abdomens were isolated by bisecting mosquitoes on the
506 transverse plane along the thoraco-abdominal junction.

507 To isolate RNA from hearts or abdomens, samples were homogenized in TRIzol
508 Reagent (Invitrogen, Carlsbad, CA), extracted following the TRIzol protocol, and
509 resuspended in Buffer RLT (Qiagen, Hilden, Germany) with 2% 2-mercaptoethanol. The
510 RNA was further purified using the RNeasy Micro Kit (Qiagen), DNase treated, and
511 eluted in RNase-free water. To isolate RNA from circulating hemocytes, perfused
512 hemolymph was collected in Buffer RLT and 2% 2-mercaptoethanol, and RNA was
513 isolated using the RNeasy Micro Kit as above.

514 No a priori statistical method was used to pre-determine sample sizes. The
515 number of RNAseq samples and biological replicates was determined prior to the
516 initiation of the study, and was based on our determination that three biological
517 replicates is a conservative approach to detect statistical differences (if any) in gene
518 expression. Three biological replicates were conducted; each heart sample contained
519 72 hearts, each hemolymph sample contained perfusate from 108 mosquitoes, and
520 each abdomen sample contained 36 abdomens.

521 The integrity and quantity of RNA was assessed on a 2100 Bioanalyzer (Agilent
522 Technologies, Santa Clara, CA) using an RNA 6000 Series II Nano kit for abdomen
523 samples and a Pico kit for the heart and hemolymph samples. The library for
524 sequencing was prepared using 1 μg of RNA and the NEBNext Ultra kit (New England

525 BioLabs, Ipswich, MA), according to the protocol for low-input samples. Library quality
526 and concentration were assessed using a DNA 1000 Series II kit on the 2100
527 Bioanalyzer.
528
529 *Illumina sequencing and differential gene expression analysis*
530 All 36 samples – 4 treatments, 3 tissue types and 3 replicates – were sequenced
531 across 3 lanes on an Illumina HiSeq 3000 (paired-end, 75 base pair read) at Vanderbilt
532 University's Vantage facility. Reads were mapped to the *A. gambiae* genome
533 (AgamP4.7) by STAR (Dobin et al., 2013; Giraldo-Calderón et al., 2015). The number of
534 uniquely mapped reads per sample averaged 23,698,077 (range: 18,487,153 –
535 31,487,002), which represented 94.03% of the total reads in a sample. Differential
536 expression was calculated based on reads per kilobase per million by DESeq2 (Love,
537 Huber, & Anders, 2014). Genes were considered significantly regulated at $\log_2$ fold
538 change $\geqslant$ 2 or $\log_2$ fold change $\leqslant$ -2 and the Benjamini–Hochberg adjusted $P < 0.05$.
539 RNAseq results are presented in Dataset S1, and includes read counts and log2 fold
540 changes. Using four-fold expression difference as the criterion, together with
541 experimental replication and statistical validation, is a conservative approach that is
542 proven to yield accurate and reliable results (Everaert et al., 2017). RNAseq data was
543 deposited into NCBI (https://www.ncbi.nlm.nih.gov) as SRA data PRJNA730047.
544
545 *Double-stranded RNA (dsRNA) synthesis and RNA interference (RNAi)*
546 Double-stranded RNA was synthesized for *rel2*, *caspar*, *PGRP-LA*, *JNK1* and
547 *JNK3*, and *puc*. *A. gambiae* cDNA was amplified by PCR using gene-specific primers

548 with T7 promoter tags (Figure 2–figure supplement 2). dsRNA was synthesis using the
549 MEGAscript T7 Kit (Applied Biosystems) as described (Sigle & Hillyer, 2018a; Yan &
550 Hillyer, 2019). As a negative control, dsRNA was synthesized for the non-mosquito
551 gene, *bla(Ap^R)*, using DNA from *E. coli* BL21(DE3) containing the pET-46 plasmid as
552 template (EMD Chemicals, Gibbstown, NJ) (Sigle & Hillyer, 2018a; Yan & Hillyer, 2019).
553 Two- or three-day-old mosquitoes were intrathoracically injected 300 ng of
554 dsRNA. Four days later, mosquitoes were divided into two groups for phenotypic
555 analyses: (i) uninfected and (ii) infected with GFP-*E. coli* (~16,528 CFUs). Injured
556 mosquitoes were not included in the experiments because injury does not induce
557 periostial hemocyte aggregation (King & Hillyer, 2012, 2013; Sigle & Hillyer, 2016).
558 RNAi efficiency of the targeted genes and mRNA abundance of the downstream
559 effector genes *TEP1*, *cec3* and *def1* was determined by qPCR (Yan & Hillyer, 2019).
560 Briefly, RNA was isolated using TRIzol from 10 whole bodies for each time and
561 treatment, purified, and used for cDNA synthesis using the SuperScript III First-Strand
562 Synthesis System for RT-PCR (Invitrogen) as described (Sigle & Hillyer, 2018a; Yan &
563 Hillyer, 2019). qPCR was conducted using gene-specific primers (Figure 2–figure
564 supplement 2) and Power SYBR Green PCR Master Mix (Applied Biosystems, Foster
565 City, CA) on a Bio Rad CFX Connect Real-Time Detection System (Hercules, CA).
566 Relative quantification was conducted using the $2^{-\Delta\Delta C_T}$ method, with *RpS7* as the
567 reference and *RpS17* as a control (League, Estévez-Lao, Yan, Garcia-Lopez, & Hillyer,
568 2017). Two to three biological replicates were conducted per gene, and the value for
569 each biological replicate is the average of two or three technical replicates.
570

571 *Fluorescence labeling and mosquito dissection*

572 Hemocytes were labeled with the Vybrant CM-DiI Cell-Labeling Solution
573 (Invitrogen) as we described (King & Hillyer, 2012). Briefly, live mosquitoes were
574 injected ~0.4 μL of 67 μM CM-DiI and 1.08 mM Hoechst 33342 (nuclear stain;
575 Invitrogen) in PBS, incubated at 27 °C for 20 min, and injected 16% paraformaldehyde.
576 Ten min later, abdomens were bisected along a coronal plane, and the dorsal portions
577 containing the heart and periostial hemocytes were mounted on glass slides using
578 Aqua-Poly/Mount (Polysciences; Warrington, PA).

579

580 *Microscopy and image acquisition*

581 Specimens were imaged on a Nikon Eclipse Ni-E compound microscope
582 connected to a Nikon Digital Sight DS-Qi1 camera and Advanced Research NIS
583 Elements software (Nikon, Tokyo, Japan). Z-stacks for bright field, red fluorescence
584 (hemocytes), green fluorescence (GFP-*E. coli*) and blue fluorescence (nuclei) were
585 acquired using a linear encoded Z-motor. Specific channels were selected and all
586 images within a stack were combined into a two-dimensional image using the Extended
587 Depth of Focus (EDF) function.

588

589 *Quantification of hemocytes*

590 Hemocytes, labeled with both CM-DiI and Hoechst 33342, were counted
591 manually by examining all images within a Z-stack (Yan & Hillyer, 2019). A cell was a
592 periostial hemocyte if adjacent to an ostium, and a non-periostial sessile hemocyte if
593 attached to the abdominal wall outside of a periostial region (King & Hillyer, 2012,

594 2013). Periostial hemocytes were counted within abdominal segments 2-7 (all
595 abdominal periostial regions) whereas non-periostial sessile hemocytes were only
596 counted on the tergum of segments 4 and 5. Hemocytes were not counted on the aorta,
597 the thoraco-abdominal ostia or the excurrent openings because few hemocytes are
598 there, and infection does not induce aggregation at those locations (Sigle & Hillyer,
599 2018b, 2018c). Data were analyzed by two-way ANOVA, followed by Dunnett's multiple
600 comparison test, with ds*bla(Ap^R)* mosquitoes as the reference (Prism 9, GraphPad
601 Software, San Diego, CA). Data presented for RNAi phenotypic experiments are for
602 individual mosquitoes, which were sampled across three to four biological trials. The
603 exception is experiments for PGRP-LA, where mosquitoes were sampled across two
604 biological trials.
605
606 *Quantification of GFP-E. coli and melanin at the periostial regions*
607 In NIS-Elements, each periostial region in an EDF image was delineated using
608 the ROI tool. GFP-*E. coli* at the periostial regions was calculated by measuring the area
609 of pixels with intensities above a threshold that distinguished GFP-*E. coli* from
610 background fluorescence (Yan & Hillyer, 2019). Melanin was quantified by measuring
611 the area of pixels with intensities below a threshold that distinguished dark melanized
612 areas from non-melanized areas (Yan & Hillyer, 2019). For each mosquito,
613 measurements from all ROIs were added. Data were analyzed by two-way ANOVA,
614 followed by Dunnett's multiple comparison test, with ds*bla(Ap^R)* mosquitoes as the
615 reference.
616

617 *Quantification of bacterial infection intensity*

618 Mosquitoes that were infected with tetracycline resistant GFP-*E. coli* for 4 or 24
619 hr were homogenized individually in PBS. A dilution of the homogenate was spread on
620 LB agar containing tetracycline, and plates were incubated overnight at 37 °C. The
621 CFUs were counted and used to calculate infection intensity. Data were analyzed by
622 two-way ANOVA, followed by Dunnett's multiple comparison test, with ds*bla(Ap^R)*
623 mosquitoes as the reference. For *rel2* and *caspar* RNAi mosquitoes, data were first $\log_2$
624 transformed to achieve normality, and then analyzed by two-way ANOVA.

625

626 **Acknowledgments**

627 This work was supported by U.S. National Science Foundation grants IOS-
628 1456844 and IOS-1949145 to J.F.H. The funders had no role in study design, data
629 collection and analysis, decision to publish, or preparation of the manuscript. We thank
630 S. Williams, J. Sanner, C. Meier, L. Martin and L. Jabbur for commenting on this
631 manuscript.

632

633 **Competing interests:** The authors declare that there are no conflicts or competing
634 interests.

635

636 **References**
637

638 Babcock, D. T., Brock, A. R., Fish, G. S., Wang, Y., Perrin, L., Krasnow, M. A., & Galko,
639 M. J. (2008). Circulating blood cells function as a surveillance system for
640 damaged tissue in *Drosophila* larvae. *Proc Natl Acad Sci U S A, 105*(29), 10017-
641 10022. doi:10.1073/pnas.0709951105
642 Banerjee, U., Girard, J. R., Goins, L. M., & Spratford, C. M. (2019). *Drosophila* as a
643 genetic model for hematopoiesis. *Genetics, 211*(2), 367-417.
644 doi:10.1534/genetics.118.300223
645 Bartholomay, L. C., Cho, W. L., Rocheleau, T. A., Boyle, J. P., Beck, E. T., Fuchs, J.
646 F., . . . Christensen, B. M. (2004). Description of the transcriptomes of immune
647 response-activated hemocytes from the mosquito vectors *Aedes aegypti* and
648 *Armigeres subalbatus*. *Infect Immun, 72*(7), 4114-4126.
649 doi:10.1128/IAI.72.7.4114-4126.2004
650 Baton, L. A., Robertson, A., Warr, E., Strand, M. R., & Dimopoulos, G. (2009). Genome-
651 wide transcriptomic profiling of *Anopheles gambiae* hemocytes reveals pathogen-
652 specific signatures upon bacterial challenge and *Plasmodium berghei* infection.
653 *BMC Genomics, 10*, 257. doi:10.1186/1471-2164-10-257
654 Blandin, S., & Levashina, E. A. (2004). Thioester-containing proteins and insect
655 immunity. *Mol Immunol, 40*(12), 903-908. doi:10.1016/j.molimm.2003.10.010
656 Bou Aoun, R., Hetru, C., Troxler, L., Doucet, D., Ferrandon, D., & Matt, N. (2011).
657 Analysis of thioester-containing proteins during the innate immune response of
658 *Drosophila melanogaster*. *J Innate Immun, 3*(1), 52-64. doi:10.1159/000321554
659 Boutros, M., Agaisse, H., & Perrimon, N. (2002). Sequential activation of signaling
660 pathways during innate immune responses in *Drosophila*. *Dev Cell, 3*(5), 711-
661 722. doi:10.1016/s1534-5807(02)00325-8
662 Bretscher, A., Honti, V., Binggeli, O., Burri, O., Poidevin, M., Kurucz, E., . . . Lemaitre,
663 B. (2015). The Nimrod transmembrane receptor Eater is required for hemocyte
664 attachment to the sessile compartment in *Drosophila melanogaster*. *Biol Open,*
665 *4*(3), 355-363. doi:10.1242/bio.201410595
666 Cevik, D., Acker, M., Michalski, C., & Jacobs, J. R. (2019). Pericardin, a *Drosophila*
667 collagen, facilitates accumulation of hemocytes at the heart. *Dev Biol, 454*(1), 52-
668 65. doi:10.1016/j.ydbio.2019.06.006
669 Chakrabarti, S., Dudzic, J. P., Li, X., Collas, E. J., Boquete, J. P., & Lemaitre, B. (2016).
670 Remote control of intestinal stem cell activity by haemocytes in *Drosophila*. *PLoS*
671 *Genet, 12*(5), e1006089. doi:10.1371/journal.pgen.1006089
672 Chiu, H., Ring, B. C., Sorrentino, R. P., Kalamarz, M., Garza, D., & Govind, S. (2005).
673 dUbc9 negatively regulates the Toll-NF-kappa B pathways in larval
674 hematopoiesis and drosomycin activation in *Drosophila*. *Dev Biol, 288*(1), 60-72.
675 doi:10.1016/j.ydbio.2005.08.008
676 Choi, Y. J., Fuchs, J. F., Mayhew, G. F., Yu, H. E., & Christensen, B. M. (2012). Tissue-
677 enriched expression profiles in *Aedes aegypti* identify hemocyte-specific
678 transcriptome responses to infection. *Insect Biochem Mol Biol, 42*(10), 729-738.
679 doi:10.1016/j.ibmb.2012.06.005
680 Chowdhury, A., Modahl, C., Tan, S., Xiang, B., Misse, D., Vial, T., . . . Pompon, J.
681 (2020). JNK pathway restricts DENV2, ZIKV and CHIKV infection by activating

682 complement and apoptosis in mosquito salivary glands. *Plos Pathogens, 16*(8).
683 doi:10.1371/journal.ppat.1008754
684 Dekmak, A. S., Yang, X., Zu Dohna, H., Buchon, N., & Osta, M. A. (2021). The route of
685 infection influences the contribution of key immunity genes to antibacterial
686 defense in *Anopheles gambiae*. *J Innate Immun, 13*(2), 107-126.
687 doi:10.1159/000511401
688 Destalminil-Letourneau, M., Morin-Poulard, I., Tian, Y., Vanzo, N., & Crozatier, M.
689 (2021). The vascular niche controls *Drosophila* hematopoiesis via fibroblast
690 growth factor signaling. *Elife, 10*. doi:10.7554/eLife.64672
691 Dobin, A., Davis, C. A., Schlesinger, F., Drenkow, J., Zaleski, C., Jha, S., . . . Gingeras,
692 T. R. (2013). STAR: ultrafast universal RNA-seq aligner. *Bioinformatics, 29*(1),
693 15-21. doi:10.1093/bioinformatics/bts635
694 Dong, Y., Das, S., Cirimotich, C., Souza-Neto, J. A., McLean, K. J., & Dimopoulos, G.
695 (2011). Engineered *Anopheles* immunity to *Plasmodium* infection. *PLoS Pathog,*
696 *7*(12), e1002458. doi:10.1371/journal.ppat.1002458
697 Dong, Y., Simões, M. L., & Dimopoulos, G. (2020). Versatile transgenic multistage
698 effector-gene combinations for *Plasmodium falciparum* suppression in
699 *Anopheles*. *Sci Adv, 6*(20), eaay5898. doi:10.1126/sciadv.aay5898
700 Dragojlovic-Munther, M., & Martinez-Agosto, J. A. (2013). Extracellular matrix-
701 modulated Heartless signaling in *Drosophila* blood progenitors regulates their
702 differentiation via a Ras/ETS/FOG pathway and target of rapamycin function.
703 *Dev Biol, 384*(2), 313-330. doi:10.1016/j.ydbio.2013.04.004
704 Etchegaray, J. I., Timmons, A. K., Klein, A. P., Pritchett, T. L., Welch, E., Meehan, T.
705 L., . . . McCall, K. (2012). Draper acts through the JNK pathway to control
706 synchronous engulfment of dying germline cells by follicular epithelial cells.
707 *Development, 139*(21), 4029-4039. doi:10.1242/dev.082776
708 Evans, I. R., Rodrigues, F. S., Armitage, E. L., & Wood, W. (2015). Draper/CED-1
709 mediates an ancient damage response to control inflammatory blood cell
710 migration in vivo. *Curr Biol, 25*(12), 1606-1612. doi:10.1016/j.cub.2015.04.037
711 Everaert, C., Luypaert, M., Maag, J. L. V., Cheng, Q. X., Dinger, M. E., Hellemans, J., &
712 Mestdagh, P. (2017). Benchmarking of RNA-sequencing analysis workflows
713 using whole-transcriptome RT-qPCR expression data. *Sci Rep, 7*(1), 1559.
714 doi:10.1038/s41598-017-01617-3
715 Feng, Y., Chen, L., Gao, L., Dong, L., Wen, H., Song, X., . . . Wang, J. (2021).
716 Rapamycin inhibits pathogen transmission in mosquitoes by promoting immune
717 activation. *PLoS Pathog, 17*(2), e1009353. doi:10.1371/journal.ppat.1009353
718 Frolet, C., Thoma, M., Blandin, S., Hoffmann, J., & Levashina, E. (2006). Boosting NF-
719 kappa B-dependent basal immunity of *Anopheles gambiae* aborts development
720 of *Plasmodium berghei*. *Immunity, 25*(4), 677-685.
721 doi:10.1016/j.immuni.2006.08.019
722 Garver, L. S., Bahia, A. C., Das, S., Souza-Neto, J. A., Shiao, J., Dong, Y., &
723 Dimopoulos, G. (2012). *Anopheles* Imd pathway factors and effectors in infection
724 intensity-dependent anti-*Plasmodium* action. *PLoS Pathog, 8*(6), e1002737.
725 doi:10.1371/journal.ppat.1002737

726 Garver, L. S., de Almeida Oliveira, G., & Barillas-Mury, C. (2013). The JNK pathway is a
727 key mediator of *Anopheles gambiae* antiplasmodial immunity. *PLoS Pathog, 9*(9),
728 e1003622. doi:10.1371/journal.ppat.1003622
729 Garver, L. S., Dong, Y., & Dimopoulos, G. (2009). Caspar controls resistance to
730 *Plasmodium falciparum* in diverse anopheline species. *PLoS Pathog, 5*(3),
731 e1000335. doi:10.1371/journal.ppat.1000335
732 Gendrin, M., Turlure, F., Rodgers, F. H., Cohuet, A., Morlais, I., & Christophides, G. K.
733 (2017). The peptidoglycan recognition proteins PGRPLA and PGRPLB regulate
734 *Anopheles* immunity to bacteria and affect infection by *Plasmodium*. *J Innate*
735 *Immun, 9*(4), 333-342. doi:10.1159/000452797
736 Gendrin, M., Zaidman-Rémy, A., Broderick, N. A., Paredes, J., Poidevin, M., Roussel,
737 A., & Lemaitre, B. (2013). Functional analysis of PGRP-LA in *Drosophila*
738 immunity. *PLoS One, 8*(7), e69742. doi:10.1371/journal.pone.0069742
739 Gerardo, N. M., Altincicek, B., Anselme, C., Atamian, H., Barribeau, S. M., de Vos,
740 M., . . . Vilcinskas, A. (2010). Immunity and other defenses in pea aphids,
741 *Acyrthosiphon pisum*. *Genome Biol, 11*(2), R21. doi:10.1186/gb-2010-11-2-r21
742 Ghosh, S., Singh, A., Mandal, S., & Mandal, L. (2015). Active hematopoietic hubs in
743 *Drosophila* adults generate hemocytes and contribute to immune response. *Dev*
744 *Cell, 33*(4), 478-488. doi:10.1016/j.devcel.2015.03.014
745 Giraldo-Calderón, G. I., Emrich, S. J., MacCallum, R. M., Maslen, G., Dialynas, E.,
746 Topalis, P., . . . Consortium, V. (2015). VectorBase: an updated bioinformatics
747 resource for invertebrate vectors and other organisms related with human
748 diseases. *Nucleic Acids Res, 43*(Database issue), D707-713.
749 doi:10.1093/nar/gku1117
750 Glenn, J. D., King, J. G., & Hillyer, J. F. (2010). Structural mechanics of the mosquito
751 heart and its function in bidirectional hemolymph transport. *J Exp Biol, 213*(4),
752 541-550. doi:10.1242/jeb.035014
753 Hernández-Martínez, S., Sánchez-Zavaleta, M., Brito, K., Herrera-Ortiz, A., Ons, S., &
754 Noriega, F. G. (2017). Allatotropin: A pleiotropic neuropeptide that elicits
755 mosquito immune responses. *PLoS One, 12*(4), e0175759.
756 doi:10.1371/journal.pone.0175759
757 Hillyer, J. F. (2016). Insect immunology and hematopoiesis. *Dev Comp Immunol, 58*,
758 102-118. doi:10.1016/j.dci.2015.12.006
759 Hillyer, J. F., & Christensen, B. M. (2002). Characterization of hemocytes from the
760 yellow fever mosquito, *Aedes aegypti*. *Histochem Cell Biol, 117*(5), 431-440.
761 doi:10.1007/s00418-002-0408-0
762 Hillyer, J. F., & Strand, M. R. (2014). Mosquito hemocyte-mediated immune responses.
763 *Curr Opin Insect Sci., 3*, 14-21. doi:10.1016/j.cois.2014.07.002
764 Horn, L., Leips, J., & Starz-Gaiano, M. (2014). Phagocytic ability declines with age in
765 adult *Drosophila* hemocytes. *Aging Cell, 13*(4), 719-728. doi:10.1111/acel.12227
766 Horton, A. A., Wang, B., Camp, L., Price, M. S., Arshi, A., Nagy, M., . . . Luckhart, S.
767 (2011). The mitogen-activated protein kinome from *Anopheles gambiae*:
768 identification, phylogeny and functional characterization of the ERK, JNK and p38
769 MAP kinases. *BMC Genomics, 12*, 574. doi:10.1186/1471-2164-12-574
770 Kambris, Z., Blagborough, A. M., Pinto, S. B., Blagrove, M. S., Godfray, H. C., Sinden,
771 R. E., & Sinkins, S. P. (2010). *Wolbachia* stimulates immune gene expression

772 and inhibits *plasmodium* development in *Anopheles gambiae*. *PLoS Pathog,*
773 *6*(10), e1001143. doi:10.1371/journal.ppat.1001143
774 Khan, M. B., Liew, J. W., Leong, C. S., & Lau, Y. L. (2016). Role of NF-kβ factor Rel2
775 during *Plasmodium falciparum* and bacterial infection in *Anopheles dirus*. *Parasit*
776 *Vectors, 9*(1), 525. doi:10.1186/s13071-016-1810-0
777 King, J. G. (2020). Developmental and comparative perspectives on mosquito immunity.
778 *Dev Comp Immunol, 103*, 103458. doi:10.1016/j.dci.2019.103458
779 King, J. G., & Hillyer, J. F. (2012). Infection-induced interaction between the mosquito
780 circulatory and immune systems. *PLoS Pathog, 8*(11), e1003058.
781 doi:10.1371/journal.ppat.1003058
782 King, J. G., & Hillyer, J. F. (2013). Spatial and temporal in vivo analysis of circulating
783 and sessile immune cells in mosquitoes: hemocyte mitosis following infection.
784 *BMC Biol, 11*, 55. doi:10.1186/1741-7007-11-55
785 Kocks, C., Cho, J., Nehme, N., Ulvila, J., Pearson, A., Meister, M., . . . Ezekowitz, R.
786 (2005). Eater, a transmembrane protein mediating phagocytosis of bacterial
787 pathogens in *Drosophila*. *Cell, 123*(2), 335-346. doi:10.1016/j.cell.2005.08.034
788 Krzemień, J., Dubois, L., Makki, R., Meister, M., Vincent, A., & Crozatier, M. (2007).
789 Control of blood cell homeostasis in *Drosophila* larvae by the posterior signalling
790 centre. *Nature, 446*(7133), 325-328. doi:10.1038/nature05650
791 Kwon, H., Mohammed, M., Franzén, O., Ankarklev, J., & Smith, R. C. (2021). Single-cell
792 analysis of mosquito hemocytes identifies signatures of immune cell subtypes
793 and cell differentiation. *Elife, 10*. doi:10.7554/eLife.66192
794 Kwon, H., & Smith, R. (2019). Chemical depletion of phagocytic immune cells in
795 *Anopheles gambiae* reveals dual roles of mosquito hemocytes in anti-
796 *Plasmodium* immunity. *Proc Natl Acad Sci U S A, 116*(28), 14119-14128.
797 doi:10.1073/pnas.1900147116
798 League, G. P., Estévez-Lao, T. Y., Yan, Y., Garcia-Lopez, V. A., & Hillyer, J. F. (2017).
799 *Anopheles gambiae* larvae mount stronger immune responses against bacterial
800 infection than adults: evidence of adaptive decoupling in mosquitoes. *Parasit*
801 *Vectors, 10*(1), 367. doi:10.1186/s13071-017-2302-6
802 League, G. P., & Hillyer, J. F. (2016). Functional integration of the circulatory, immune,
803 and respiratory systems in mosquito larvae: pathogen killing in the hemocyte-rich
804 tracheal tufts. *BMC Biol, 14*, 78. doi:10.1186/s12915-016-0305-y
805 Leitão, A. B., & Sucena, É. (2015). *Drosophila* sessile hemocyte clusters are true
806 hematopoietic tissues that regulate larval blood cell differentiation. *Elife, 4*.
807 doi:10.7554/eLife.06166
808 Levashina, E. A., Moita, L. F., Blandin, S., Vriend, G., Lagueux, M., & Kafatos, F. C.
809 (2001). Conserved role of a complement-like protein in phagocytosis revealed by
810 dsRNA knockout in cultured cells of the mosquito, *Anopheles gambiae*. *Cell,*
811 *104*(5), 709-718. doi:10.1016/s0092-8674(01)00267-7
812 Love, M. I., Huber, W., & Anders, S. (2014). Moderated estimation of fold change and
813 dispersion for RNA-seq data with DESeq2. *Genome Biol, 15*(12), 550.
814 doi:10.1186/s13059-014-0550-8
815 Luna, C., Hoa, N. T., Lin, H., Zhang, L., Nguyen, H. L., Kanzok, S. M., & Zheng, L.
816 (2006). Expression of immune responsive genes in cell lines from two different

817 Anopheline species. *Insect Mol Biol, 15*(6), 721-729. doi:10.1111/j.1365-
818 2583.2006.00661.x
819 Ma, L., Liu, L., Zhao, Y., Yang, L., Chen, C., Li, Z., & Lu, Z. (2020). JNK pathway plays
820 a key role in the immune system of the pea aphid and is regulated by microRNA-
821 184. *PLoS Pathog, 16*(6), e1008627. doi:10.1371/journal.ppat.1008627
822 Macdonald, J. M., Doherty, J., Hackett, R., & Freeman, M. R. (2013). The c-Jun kinase
823 signaling cascade promotes glial engulfment activity through activation of draper
824 and phagocytic function. *Cell Death Differ, 20*(9), 1140-1148.
825 doi:10.1038/cdd.2013.30
826 Manaka, J., Kuraishi, T., Shiratsuchi, A., Nakai, Y., Higashida, H., Henson, P., &
827 Nakanishi, Y. (2004). Draper-mediated and phosphatidylserine-independent
828 phagocytosis of apoptotic cells by *Drosophila* hemocytes/macrophages. *J Biol*
829 *Chem, 279*(46), 48466-48476. doi:10.1074/jbc.M408597200
830 Mantuano, E., Jo, M., Gonias, S. L., & Campana, W. M. (2010). Low density lipoprotein
831 receptor-related protein (LRP1) regulates Rac1 and RhoA reciprocally to control
832 Schwann cell adhesion and migration. *J Biol Chem, 285*(19), 14259-14266.
833 doi:10.1074/jbc.M109.085126
834 Meister, S., Agianian, B., Turlure, F., Relógio, A., Morlais, I., Kafatos, F. C., &
835 Christophides, G. K. (2009). *Anopheles gambiae* PGRPLC-mediated defense
836 against bacteria modulates infections with malaria parasites. *PLoS Pathog, 5*(8),
837 e1000542. doi:10.1371/journal.ppat.1000542
838 Meister, S., Kanzok, S. M., Zheng, X. L., Luna, C., Li, T. R., Hoa, N. T., . . . Zheng, L.
839 (2005). Immune signaling pathways regulating bacterial and malaria parasite
840 infection of the mosquito *Anopheles gambiae*. *Proc Natl Acad Sci U S A,*
841 *102*(32), 11420-11425. doi:10.1073/pnas.0504950102
842 Mesquita, R. D., Vionette-Amaral, R. J., Lowenberger, C., Rivera-Pomar, R., Monteiro,
843 F. A., Minx, P., . . . Oliveira, P. L. (2015). Genome of *Rhodnius prolixus*, an insect
844 vector of Chagas disease, reveals unique adaptations to hematophagy and
845 parasite infection. *Proc Natl Acad Sci U S A, 112*(48), 14936-14941.
846 doi:10.1073/pnas.1506226112
847 Minakhina, S., Tan, W., & Steward, R. (2011). JAK/STAT and the GATA factor Pannier
848 control hemocyte maturation and differentiation in *Drosophila*. *Dev Biol, 352*(2),
849 308-316. doi:10.1016/j.ydbio.2011.01.035
850 Mitri, C., Jacques, J. C., Thiery, I., Riehle, M. M., Xu, J., Bischoff, E., . . . Bourgouin, C.
851 (2009). Fine pathogen discrimination within the APL1 gene family protects
852 *Anopheles gambiae* against human and rodent malaria species. *PLoS Pathog,*
853 *5*(9), e1000576. doi:10.1371/journal.ppat.1000576
854 Moita, L. F., Vriend, G., Mahairaki, V., Louis, C., & Kafatos, F. C. (2006). Integrins of
855 *Anopheles gambiae* and a putative role of a new beta integrin, BINT2, in
856 phagocytosis of *E. coli*. *Insect Biochem Mol Biol, 36*(4), 282-290.
857 doi:10.1016/j.ibmb.2006.01.004
858 Moita, L. F., Wang-Sattler, R., Michel, K., Zimmermann, T., Blandin, S., Levashina, E.
859 A., & Kafatos, F. C. (2005). In vivo identification of novel regulators and
860 conserved pathways of phagocytosis in *A. gambiae*. *Immunity, 23*(1), 65-73.
861 doi:10.1016/j.immuni.2005.05.006

Myllymäki, H., Valanne, S., & Rämet, M. (2014). The *Drosophila* imd signaling pathway. *J Immunol, 192*(8), 3455-3462. doi:10.4049/jimmunol.1303309

Márkus, R., Laurinyecz, B., Kurucz, E., Honti, V., Bajusz, I., Sipos, B., . . . Andó, I. (2009). Sessile hemocytes as a hematopoietic compartment in *Drosophila melanogaster*. *Proc Natl Acad Sci U S A, 106*(12), 4805-4809. doi:10.1073/pnas.0801766106

Nagaosa, K., Okada, R., Nonaka, S., Takeuchi, K., Fujita, Y., Miyasaka, T., . . . Nakanishi, Y. (2011). Integrin βv-mediated phagocytosis of apoptotic cells in *Drosophila* embryos. *J Biol Chem, 286*(29), 25770-25777. doi:10.1074/jbc.M110.204503

Nishide, Y., Kageyama, D., Yokoi, K., Jouraku, A., Tanaka, H., Futahashi, R., & Fukatsu, T. (2019). Functional crosstalk across IMD and Toll pathways: insight into the evolution of incomplete immune cascades. *Proc Biol Sci, 286*(1897), 20182207. doi:10.1098/rspb.2018.2207

Nsango, S., Pompon, J., Xie, T., Rademacher, A., Fraiture, M., Thoma, M., . . . Levashina, E. (2013). AP-1/Fos-TGase2 axis mediates wounding-induced *Plasmodium falciparum* killing in *Anopheles gambiae*. *J Biol Chem, 288*(22), 16145-16154. doi:10.1074/jbc.M112.443267

Peirce, M. J., Mitchell, S. N., Kakani, E. G., Scarpelli, P., South, A., Shaw, W. R., . . . Catteruccia, F. (2020). JNK signaling regulates oviposition in the malaria vector *Anopheles gambiae*. *Sci Rep, 10*(1), 14344. doi:10.1038/s41598-020-71291-5

Pinto, S. B., Lombardo, F., Koutsos, A. C., Waterhouse, R. M., McKay, K., An, C., . . . Michel, K. (2009). Discovery of *Plasmodium* modulators by genome-wide analysis of circulating hemocytes in *Anopheles gambiae*. *Proc Natl Acad Sci U S A, 106*(50), 21270-21275. doi:10.1073/pnas.0909463106

Qiu, P., Pan, P. C., & Govind, S. (1998). A role for the *Drosophila* Toll/Cactus pathway in larval hematopoiesis. *Development, 125*(10), 1909-1920. doi:10.1242/dev.125.10.1909

Rabiej, V. K., Pflanzner, T., Wagner, T., Goetze, K., Storck, S. E., Eble, J. A., . . . Pietrzik, C. U. (2016). Low density lipoprotein receptor-related protein 1 mediated endocytosis of β1-integrin influences cell adhesion and cell migration. *Exp Cell Res, 340*(1), 102-115. doi:10.1016/j.yexcr.2015.11.020

Raddi, G., Barletta, A. B. F., Efremova, M., Ramirez, J. L., Cantera, R., Teichmann, S. A., . . . Billker, O. (2020). Mosquito cellular immunity at single-cell resolution. *Science, 369*(6507), 1128-1132. doi:10.1126/science.abc0322

Ramphul, U., Garver, L., Molina-Cruz, A., Canepa, G., & Barillas-Mury, C. (2015). *Plasmodium falciparum* evades mosquito immunity by disrupting JNK-mediated apoptosis of invaded midgut cells. *Proc Natl Acad Sci U S A, 112*(5), 1273-1280. doi:10.1073/pnas.1423586112

Rani, J., Chauhan, C., Das De, T., Kumari, S., Sharma, P., Tevatiya, S., . . . Dixit, R. (2021). Hemocyte RNA-Seq analysis of Indian malarial vectors *Anopheles stephensi* and *Anopheles culicifacies*: From similarities to differences. *Gene, 798*, 145810. doi:10.1016/j.gene.2021.145810

Rämet, M., Manfruelli, P., Pearson, A., Mathey-Prevot, B., & Ezekowitz, R. A. (2002). Functional genomic analysis of phagocytosis and identification of a *Drosophila* receptor for *E. coli*. *Nature, 416*(6881), 644-648. doi:10.1038/nature735

908 Salcedo-Porras, N., Guarneri, A., Oliveira, P. L., & Lowenberger, C. (2019). *Rhodnius*
909 *prolixus*: Identification of missing components of the IMD immune signaling
910 pathway and functional characterization of its role in eliminating bacteria. *PLoS*
911 *One, 14*(4), e0214794. doi:10.1371/journal.pone.0214794
912 Schmid, M. R., Anderl, I., Vo, H. T., Valanne, S., Yang, H., Kronhamn, J., . . . Hultmark,
913 D. (2016). Genetic screen in *Drosophila* larvae links *ird1* function to Toll signaling
914 in the fat body and hemocyte motility. *PLoS One, 11*(7), e0159473.
915 doi:10.1371/journal.pone.0159473
916 Schnitger, A. K., Kafatos, F. C., & Osta, M. A. (2007). The melanization reaction is not
917 required for survival of *Anopheles gambiae* mosquitoes after bacterial infections.
918 *J Biol Chem, 282*(30), 21884-21888. doi:10.1074/jbc.M701635200
919 Severo, M., Landry, J., Lindquist, R., Goosmann, C., Brinkmann, V., Collier, P., . . .
920 Levashina, E. (2018). Unbiased classification of mosquito blood cells by single-
921 cell genomics and high-content imaging. *Proc Natl Acad Sci U S A, 115*(32),
922 E7568-E7577. doi:10.1073/pnas.1803062115
923 Shaw, W. R., & Catteruccia, F. (2019). Vector biology meets disease control: using
924 basic research to fight vector-borne diseases. *Nat Microbiol, 4*(1), 20-34.
925 doi:10.1038/s41564-018-0214-7
926 Shibata, T., Sekihara, S., Fujikawa, T., Miyaji, R., Maki, K., Ishihara, T., . . . Kawabata,
927 S. (2013). Transglutaminase-catalyzed protein-protein cross-linking suppresses
928 the activity of the NF-κB-like transcription factor relish. *Sci Signal, 6*(285), ra61.
929 doi:10.1126/scisignal.2003970
930 Sigle, L. T., & Hillyer, J. F. (2016). Mosquito hemocytes preferentially aggregate and
931 phagocytose pathogens in the periostial regions of the heart that experience the
932 most hemolymph flow. *Dev Comp Immunol, 55*, 90-101.
933 doi:10.1016/j.dci.2015.10.018
934 Sigle, L. T., & Hillyer, J. F. (2018a). *Eater* and *draper* are involved in the periostial
935 haemocyte immune response in the mosquito *Anopheles gambiae*. *Insect Mol*
936 *Biol, 27*(4), 429-438. doi:10.1111/imb.12383
937 Sigle, L. T., & Hillyer, J. F. (2018b). Mosquito hemocytes associate with circulatory
938 structures that support intracardiac retrograde hemolymph flow. *Front Physiol, 9*,
939 1187. doi:10.3389/fphys.2018.01187
940 Sigle, L. T., & Hillyer, J. F. (2018c). Structural and functional characterization of the
941 contractile aorta and associated hemocytes of the mosquito. *J Exp Biol, 221*(Pt
942 12). doi:10.1242/jeb.181107
943 Silverman, N., Zhou, R., Erlich, R. L., Hunter, M., Bernstein, E., Schneider, D., &
944 Maniatis, T. (2003). Immune activation of NF-kappaB and JNK requires
945 *Drosophila* TAK1. *J Biol Chem, 278*(49), 48928-48934.
946 doi:10.1074/jbc.M304802200
947 Somogyi, K., Sipos, B., Pénzes, Z., Kurucz, E., Zsámboki, J., Hultmark, D., & Andó, I.
948 (2008). Evolution of genes and repeats in the Nimrod superfamily. *Mol Biol Evol,*
949 *25*(11), 2337-2347. doi:10.1093/molbev/msn180
950 Souvannaseng, L., Hun, L. V., Baker, H., Klyver, J. M., Wang, B., Pakpour, N., . . .
951 Luckhart, S. (2018). Inhibition of JNK signaling in the Asian malaria vector
952 *Anopheles stephensi* extends mosquito longevity and improves resistance to

953 *Plasmodium falciparum* infection. *PLoS Pathog, 14*(11), e1007418.
954 doi:10.1371/journal.ppat.1007418
955 Strand, M. (2008). The insect cellular immune response. *Insect Sci, 15*(1), 1-14.
956 doi:10.1111/j.1744-7917.2008.00183.x
957 Thomas, T., De, T. D., Sharma, P., Lata, S., Saraswat, P., Pandey, K. C., & Dixit, R.
958 (2016). Hemocytome: deep sequencing analysis of mosquito blood cells in Indian
959 malarial vector *Anopheles stephensi*. *Gene, 585*(2), 177-190.
960 doi:10.1016/j.gene.2016.02.031
961 Weavers, H., Evans, I. R., Martin, P., & Wood, W. (2016). Corpse engulfment generates
962 a molecular memory that primes the macrophage inflammatory response. *Cell,*
963 *165*(7), 1658-1671. doi:10.1016/j.cell.2016.04.049
964 Werner, T., Liu, G., Kang, D., Ekengren, S., Steiner, H., & Hultmark, D. (2000). A family
965 of peptidoglycan recognition proteins in the fruit fly *Drosophila melanogaster*.
966 *Proc Natl Acad Sci U S A, 97*(25), 13772-13777. doi:10.1073/pnas.97.25.13772
967 Williams, M. J., Wiklund, M. L., Wikman, S., & Hultmark, D. (2006). Rac1 signalling in
968 the *Drosophila* larval cellular immune response. *J Cell Sci, 119*(Pt 10), 2015-
969 2024. doi:10.1242/jcs.02920
970 Wong, C. O., Gregory, S., Hu, H., Chao, Y., Sepúlveda, V. E., He, Y., . . .
971 Venkatachalam, K. (2017). Lysosomal degradation is required for sustained
972 phagocytosis of bacteria by macrophages. *Cell Host Microbe, 21*(6), 719-
973 730.e716. doi:10.1016/j.chom.2017.05.002
974 Yan, Y., & Hillyer, J. F. (2019). Complement-like proteins TEP1, TEP3 and TEP4 are
975 positive regulators of periostial hemocyte aggregation in the mosquito *Anopheles*
976 *gambiae*. *Insect Biochem Mol Biol, 107*, 1-9. doi:10.1016/j.ibmb.2019.01.007
977 Yan, Y., & Hillyer, J. F. (2020). The immune and circulatory systems are functionally
978 integrated across insect evolution. *Sci Adv, 6*(48). doi:10.1126/sciadv.abb3164
979 Zettervall, C. J., Anderl, I., Williams, M. J., Palmer, R., Kurucz, E., Ando, I., & Hultmark,
980 D. (2004). A directed screen for genes involved in *Drosophila* blood cell
981 activation. *Proc Natl Acad Sci U S A, 101*(39), 14192-14197.
982 doi:10.1073/pnas.0403789101
983 Zhuang, Z. H., Sun, L., Kong, L., Hu, J. H., Yu, M. C., Reinach, P., . . . Ge, B. X. (2006).
984 *Drosophila* TAB2 is required for the immune activation of JNK and NF-kappaB.
985 *Cell Signal, 18*(7), 964-970. doi:10.1016/j.cellsig.2005.08.020
986

987 **Figure supplements:**

988

989 **Figure 1–figure supplement 1.** Upregulated genes in the heart with periostial

990 hemocytes at 4 hr following both GFP-*E. coli* and *S. aureus* infection.

			***E. coli* vs Injured**		***S. aureus* vs Injured**	
Gene ID	**Gene name**	**Gene description (if annotated)**	**Log2Foldchange**	**Adjusted P**	**Log2Foldchange**	**Adjusted P**
AGAP000694	*cec3*	cecropin anti-microbial peptide	2.72	8E-14	3.20	2E-19
AGAP000786			2.88	4E-06	3.12	2E-07
AGAP001160			3.03	3E-21	4.46	1E-47
AGAP001212	*PGRPLB*	peptidoglycan recognition protein (long)	3.10	2E-25	4.21	3E-47
AGAP001508			3.19	4E-07	5.03	2E-17
AGAP001563		glycerol kinase	2.58	7E-12	2.70	3E-13
AGAP001597			2.14	9E-04	2.14	6E-04
AGAP001610			4.07	2E-21	4.13	2E-22
AGAP001634			3.52	1E-14	2.48	1E-07
AGAP001648	*CLIPB17*	CLIP-domain serine protease	2.24	4E-10	3.01	3E-18
AGAP001828			2.13	2E-16	2.38	9E-21
AGAP002064			2.05	7E-18	2.29	1E-22
AGAP002065		alpha-tocopherol transfer protein	2.14	1E-13	2.64	3E-21
AGAP002291		ebony	2.81	1E-30	3.62	2E-51
AGAP002323			2.82	2E-11	3.31	4E-16
AGAP002331	*esp*	sodium-independent sulfate anion transporter	3.15	8E-20	2.94	1E-17
AGAP002359		carbonic anhydrase	2.62	2E-02	4.62	4E-06
AGAP002536			2.48	3E-13	2.75	1E-16
AGAP002883			2.28	3E-24	2.69	5E-34
AGAP003488		nucleotide exchange factor SIL1	2.02	2E-06	2.49	1E-09
AGAP004170			2.18	4E-21	2.73	8E-34
AGAP004181		Fibroblast growth factor	2.53	1E-06	2.40	4E-06
AGAP004826			3.04	4E-09	4.30	2E-18
AGAP005205	*PGRPLA*	peptidoglycan recognition protein (long)	2.36	7E-47	2.66	1E-60
AGAP005610			2.44	1E-06	4.99	2E-27
AGAP005839		MFS transporter, FLVCR family	3.65	4E-41	3.97	3E-49
AGAP006426		cyanogenic beta-glucosidase	2.65	2E-03	5.58	2E-13
AGAP006670		gamma-glutamyl hydrolase	2.31	8E-24	2.90	4E-38
AGAP006671			3.18	6E-18	3.85	2E-27
AGAP006674		chymotrypsin-like protease (Precursor)	2.93	2E-02	7.46	1E-12
AGAP006745			2.35	4E-29	2.78	3E-41
AGAP006747	*rel2*	NF-kappaB Relish-like transcription factor	2.00	2E-33	2.21	3E-41
AGAP007659			2.61	4E-15	3.57	1E-28
AGAP008279	*d7l2*	D7 long form salivary protein	16.43	2E-05	13.73	3E-04
AGAP008851		E3 ubiquitin-protein ligase mind-bomb	2.66	2E-26	2.95	8E-33
AGAP009091	*ddc*	dopa decarboxylase	3.96	2E-50	4.81	3E-75
AGAP009099	*TGase3*	Transglutaminase	3.98	2E-17	4.05	1E-18
AGAP009100	*TGase1*	Transglutaminase	3.20	3E-37	3.76	1E-51
AGAP009145			2.12	1E-13	3.03	4E-28
AGAP009213	*SRPN16*	serine protease inhibitor (serpin) 16	2.61	8E-13	3.75	1E-26
AGAP009214	*CLIPB11*	CLIP-domain serine protease	2.13	1E-06	3.71	2E-19
AGAP009460	*JNK3*	c-Jun N-terminal kinase	2.22	1E-04	3.47	1E-10
AGAP009985		4-nitrophenylphosphatase	2.19	3E-08	3.16	4E-17
AGAP010197		SPRY domain-containing SOCS box protein 1	2.31	2E-20	2.85	2E-31
AGAP010398		Flavin-containing monooxygenase FMO GS-OX-like 1	2.78	8E-08	5.85	1E-33
AGAP010934			2.94	1E-30	3.17	3E-36
AGAP011294	*def1*	defensin anti-microbial peptide	2.13	2E-05	2.70	1E-08
AGAP011326	*IAP2*	inhibitor of apoptosis 2	3.21	2E-38	3.29	1E-40
AGAP011588			2.60	2E-29	3.33	4E-49
AGAP011654		membrane dipeptidase	2.13	5E-05	3.58	3E-13
AGAP011764			2.71	5E-63	2.87	4E-71
AGAP011992		lysosomal acid lipase	2.72	7E-05	3.01	4E-06
AGAP012166			3.70	2E-13	2.92	8E-09
AGAP013506	*upd3a*	JAK/STAT pathway cytokine unpaired 3 variant A	3.89	2E-12	4.05	8E-14
AGAP028615	*nat5*	nutrient amino acid transporter 5	2.54	4E-10	4.28	2E-28

991
992

993 **Figure 1–figure supplement 2.** Upregulated genes in the circulating hemocytes at 4 hr

994 following both GFP-*E. coli* and *S. aureus* infection.

			***E. coli* vs Injured**		***S. aureus* vs Injured**	
Gene ID	**Gene name**	**Gene description (if annotated)**	**Log2Foldchange**	**Adjusted P**	**Log2Foldchange**	**Adjusted P**
AGAP000899			3.31	3E-07	4.74	8E-16
AGAP001212	*PGRPLB*	peptidoglycan recognition protein (long)	2.68	2E-18	4.39	4E-51
AGAP001430			2.27	2E-18	3.39	7E-43
AGAP001508			2.06	3E-03	3.26	1E-07
AGAP002291		ebony	2.46	3E-23	3.73	2E-55
AGAP004115		cystinosin	2.07	5E-03	5.38	5E-18
AGAP005610			2.45	8E-08	4.09	7E-23
AGAP005639	*abcb2*	ATP-binding cassette transporter (ABC transporter) family B member 2	2.23	1E-12	3.47	1E-31
AGAP007651		growth arrest and DNA-damage-inducible protein	2.19	8E-11	3.30	2E-25
AGAP009091	*ddc*	dopa decarboxylase	2.06	2E-13	2.93	3E-28
AGAP010349			2.28	3E-05	3.50	1E-12
AGAP010387		alanine-glyoxylate aminotransferase	2.29	3E-03	3.54	3E-07
AGAP010571			2.43	5E-06	3.25	3E-11
AGAP010855		solute carrier family 45, member 1/2/4	3.24	7E-06	5.23	7E-16
AGAP011326	*IAP2*	inhibitor of apoptosis 2	2.26	2E-18	2.58	4E-25
AGAP011391			2.07	7E-07	3.62	8E-22
AGAP011588			2.43	7E-25	3.18	8E-45
AGAP011589			2.95	2E-02	3.46	3E-03
AGAP012565			3.58	7E-02	3.78	5E-02
AGAP013285	*ir7u*	ionotropic receptor IR7u	2.36	3E-03	3.46	9E-07
AGAP028615	*nat5*	nutrient amino acid transporter 5	2.27	9E-08	4.06	2E-25

995
996
997
998 **Figure 1–figure supplement 3.** Upregulated genes in the abdomen at 4 hr following

999 both GFP-*E. coli* and *S. aureus* infection.

			***E. coli* vs Injured**		***S. aureus* vs Injured**	
Gene ID	**Gene name**	**Gene description (if annotated)**	**Log2Foldchange**	**Adjusted P**	**Log2Foldchange**	**Adjusted P**
AGAP001212	*PGRPLB*	peptidoglycan recognition protein (long)	3.22	4E-26	3.97	8E-41
AGAP001508			2.54	3E-04	4.63	5E-14
AGAP001610			3.33	1E-13	2.75	1E-09
AGAP001648	*CLIPB17*	CLIP-domain serine protease	2.04	8E-08	3.27	1E-20
AGAP002291		ebony	2.52	3E-24	2.47	1E-23
AGAP006670		gamma-glutamyl hydrolase	2.08	1E-18	2.33	9E-24
AGAP006745			2.06	8E-21	2.39	2E-28
AGAP007651		growth arrest and DNA-damage-inducible protein	2.17	2E-10	2.16	1E-10
AGAP007659			2.13	2E-09	2.45	7E-13
AGAP009145			2.18	2E-13	3.51	2E-36
AGAP010398		Flavin-containing monooxygenase FMO GS-OX-like 1	2.62	2E-06	5.93	3E-33
AGAP010934			2.59	6E-23	2.25	1E-17
AGAP011294	*def1*	defensin anti-microbial peptide	2.04	2E-04	2.39	3E-06
AGAP011326	*IAP2*	inhibitor of apoptosis 2	2.16	2E-16	2.17	8E-17
AGAP013348			2.40	4E-22	3.34	2E-43

1000
1001
1002
1003
1004
1005
1006

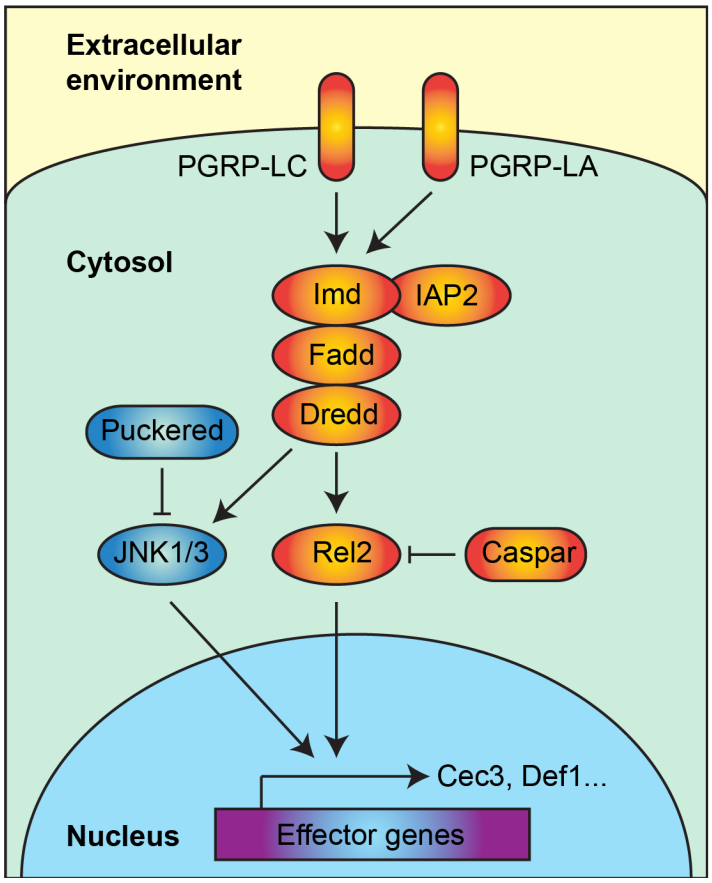

1007
1008
1009 **Figure 1–figure supplement 4. The IMD and interlinked JNK pathways are two of**
1010 **the major immune pathways in mosquitoes.** The activation of PGRP-LC triggers the
1011 IMD signaling pathway, which includes IAP2, imd, fadd and dredd. This activation
1012 dissociates the transcription factor, rel2, from the inhibitor protein, caspar. Rel2 then
1013 translocates into the nucleus and induces the production of effectors such as cec3 and
1014 def1. Although PGRP-LC is the canonical activator of the IMD pathway, PGRP-LA has
1015 also been implicated as an upstream activator of this immune pathway. The IMD
1016 pathway bifurcates into the JNK pathway, which activates JNK1 and JNK3, and induces
1017 the expression of effector genes. The JNK pathway is negatively regulated by puckered.
1018
1019
1020
1021

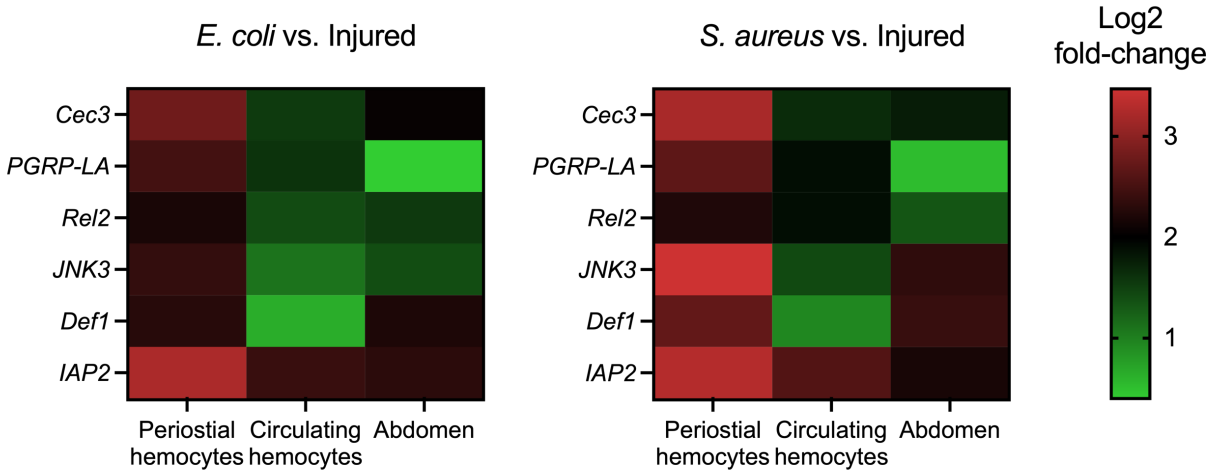

Figure 1–figure supplement 5. IMD and JNK pathway genes are more highly upregulated after infection in the heart and periostial hemocytes than in the circulating hemocytes or the abdomen. Heat map showing that all six IMD and JNK pathway genes identified in our unbiased screen are more highly upregulated after *E. coli* and *S. aureus* infection in the heart and periostial hemocytes than in the other tissues.

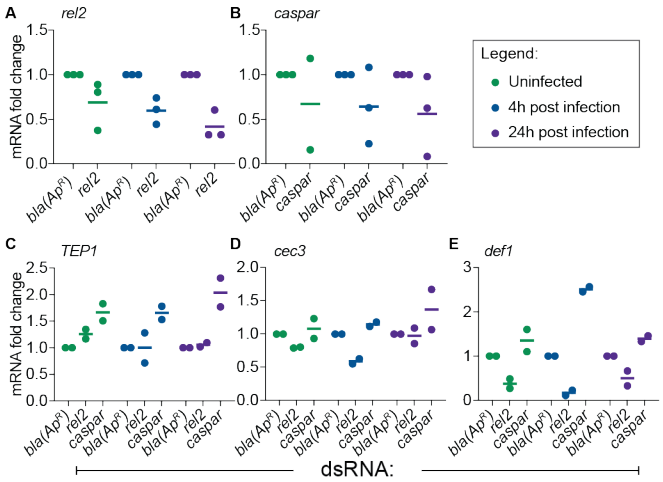

Figure 2–figure supplement 1. RNA interference-mediated gene silencing of *rel2* and *caspar* reduces their mRNA abundance while altering the mRNA abundance of *TEP1*, *cec3* and *def1*. Relative mRNA abundance of *rel2* (A), *caspar* (B), *TEP1* (C), *cec3* (D), and *def1* (E) in mosquitoes injected ds*bla(Ap^R)*, ds*rel2* or ds*caspar*. mRNA abundance was measured in mosquitoes that were not infected or had been infected with GFP-*E. coli* for 4 or 24 hr. Horizontal line, mean; Circles, individual biological trials. Data are relative to mRNA abundance in the ds*bla(Ap^R)* group of that specific trial and treatment.

1043 **Figure 2–figure supplement 2.** Gene names, gene IDs, and primers used.

Application	Gene	dsRNA	VectorBase ID[a]	Primer sequence (forward and reverse) [b]
qPCR	*Rps7*		AGAP010592	GACGGATCCCAGCTGATAAA
qPCR				GTTCTCTGGGAATTCGAACG
qPCR	*Rps17*		AGAP004887	GACGAAACCACTGCGTAACA
qPCR				TGCTCCAGTGCTGAAACATC
qPCR	*rel2*		AGAP006747	TTCGCTGCTCGACTTTCACT
qPCR				CCAACCGAAGGCAGCAAATC
qPCR	*caspar*		AGAP006473	TCGTAGCCAATGCGAAGTGT
qPCR				TCGTTCGTTCTCTTCACGCA
qPCR	*PGRP-LA-RA*		AGAP005205	GGCAATGGCGGAAATACGAC
qPCR				GGTTCCGCTGAAGGTAGTCC
qPCR	*PGRP-LA-RB*		AGAP005205	GGTACGTTTGACGCGGATC
qPCR				GTCCGCGGTTCTGATTGTT
qPCR	*PGRP-LA-RC*		AGAP005205	GCAATGGCGGAAATACGAC
qPCR				ATGCCCGGCGAAGTATATG
qPCR	*JNK1*		AGAP029555[c]	TGTTTCCGACCGACTCGAA
qPCR				CGTCCACGCTGTGATCGTA
qPCR	*JNK3*		AGAP009460	ACAGTCTTAAGCATCCCGGC
qPCR				GCGGCAAAACACACTCCTTT
qPCR	*puckered*		AGAP004353	ATTCAACGGAGGTCGATTTG
qPCR				AACTTTCTAGCCCCCATCGT
qPCR	*TEP1*		AGAP010815	GACGTCCAAATACGGATCTCA
qPCR				CTTTCAGGCATCACCCGTAT
qPCR	*cec3*		AGAP000694	TTCCCAGTGCATCTGTGTCC
qPCR				GAGCTTTGTAGCCGGCAATG
qPCR	*def1*		AGAP011294	GCAACGATCGTCTGTACCATT
qPCR				GCTTGGCCCGATAGTTCTC
RNAi	*bla(Ap^R)*	ds*bla(Ap^R)*	(Bacterial gene)	TAATACGACTCACTATAGGGCCGAGCGCAGAAGTGGT
RNAi				TAATACGACTCACTATAGGGAACCGGAGCTGAATGAA
RNAi	*rel2*	ds*rel2*	AGAP006747	TAATACGACTCACTATACGGAGAAGTCGAAGAAAACG
RNAi				TAATACGACTCACTATACACAGGCACACCTGATTGAG
RNAi	*caspar*	ds*caspar*	AGAP006473	TAATACGACTCACTATAGGGACAGAAGGCCGCTTT
RNAi				TAATACGACTCACTATAGGGAGTGGTGGTGCAGAGTT
RNAi	*PGRP-LA*	ds*PGRP-LA-RARB* [d]	AGAP005205	TAATACGACTCACTATAGGGAGATACTGTTCGACACCA
RNAi				TAATACGACTCACTATAGGGCTGGCTGTGGTAGGTTT
RNAi	*PGRP-LA*	ds*PGRP-LA-RC*	AGAP005205	TAATACGACTCACTATAGGGCACATGGTCATCGATC
RNAi				TAATACGACTCACTATAGGGATCGATTTTGGGTATTC
RNAi	*JNK1/JNK3*	ds*JNK1/3* [e]	AGAP0290555 /AGAP009460	TAATACGACTCACTATAGGGGTCACGCCTTCTACACCGTC
RNAi				TAATACGACTCACTATAGGGCAGCCCAAAGTCGAGGATT
RNAi	*puc*	ds*puc*	AGAP004353	TAATACGACTCACTATAGGGTGAAACATAAATCGCCCTGC
RNAi				TAATACGACTCACTATAGGGGACAGACCCTTGTAGCGCAT

1044
1045 a Vectorbase IDs were obtained from the AgamP4 assembly in www.vectorbase.org (exception: *bla(Ap^R)*).
1046 b Underlined sequences are specific to the T7 RNA polymerase promoter sites needed for dsRNA synthesis.
1047 c Previous gene ID of JNK1 is AGAP009461.
1048 d ds*PGRP-LA-RARB* targets both the RA and RB splice variants of *PGRP-LA*.
1049 e ds*JNK1/3* targets both *JNK1* and *JNK3*.
1050
1051

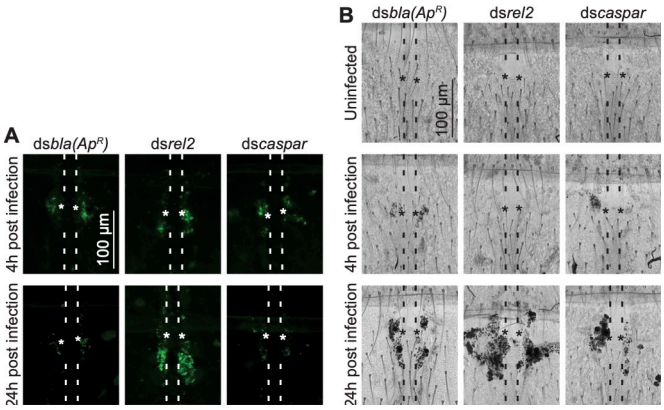

1052
1053
1054 **Figure 2–figure supplement 3. The IMD pathway affects GFP-*E. coli* and melanin**
1055 **accumulation at the periostial regions.** (*A*) Fluorescence images show the
1056 accumulation of GFP-*E. coli* (green) around a single pair of ostia (asterisks) on a
1057 segment of the heart (outlined by dotted lines) of ds*bla(Ap^R)*, ds*rel2* and ds*caspar*
1058 mosquitoes that had been infected with GFP-*E. coli* for 4 or 24 hr. (*B*) Bright field
1059 images show the accumulation of melanin (dark deposits) around a single pair of ostia
1060 (asterisks) on a segment of the heart (outlined by dotted lines) of ds*bla(Ap^R)*, ds*rel2* and
1061 ds*caspar* mosquitoes that were not infected or had been infected with GFP-*E. coli* for 4
1062 or 24 hr. Anterior is on top. Quantification of all mosquitoes assayed is presented in
1063 figures 2D and 2E.
1064
1065
1066

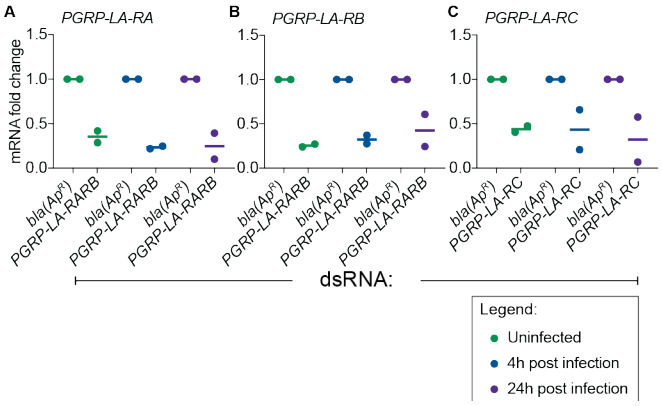

1067
1068
1069 **Figure 3–figure supplement 1. RNA interference-mediated gene silencing of**
1070 ***PGRP-LA* reduces the mRNA abundance of all splice variants.** Relative mRNA
1071 abundance of *PGRP-LA-RA* (A), *PGRP-LA-RB* (B) and *PGRP-LA-RC* (C) in mosquitoes
1072 injected ds*bla(Ap^R)*, ds*PGRP-LA-RARB* or ds*PGRP-LA-RC*. mRNA abundance was
1073 measured in mosquitoes that were not infected or had been infected with GFP-*E. coli*
1074 for 4 or 24 hr. Horizontal line, mean; Circles, individual biological trials. Data are relative
1075 to mRNA abundance in the ds*bla(Ap^R)* group of that specific trial and treatment.
1076

1077

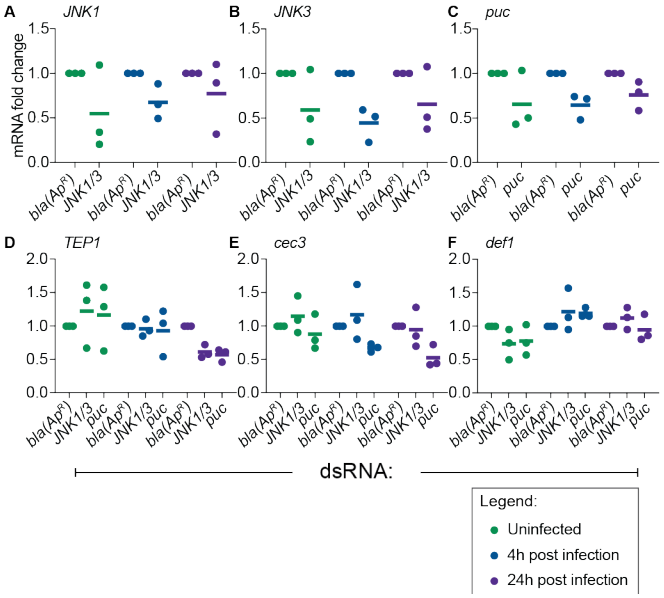

1078
1079
1080 **Figure 4–figure supplement 1. RNA interference-mediated gene silencing of *JNK1*,**
1081 ***JNK3* and *puc* reduces their mRNA abundance while having a limited impact on**
1082 **the mRNA abundance of *TEP1*, *cec3* and *def1*.** Relative mRNA abundance of *JNK1*
1083 (A), *JNK3* (B), *puc* (C), *TEP1* (D), *cec3* (E), and *def1* (F) in mosquitoes injected
1084 ds*bla(Ap^R),* ds*JNK1/3* or ds*puc*. mRNA abundance was measured in mosquitoes that
1085 were not infected or had been infected with GFP-*E. coli* for 4 or 24 hr. Horizontal line,
1086 mean; Circles, individual biological trials. Data are relative to mRNA abundance in the
1087 ds*bla(Ap^R)* group of that specific trial and treatment.
1088
1089

1090

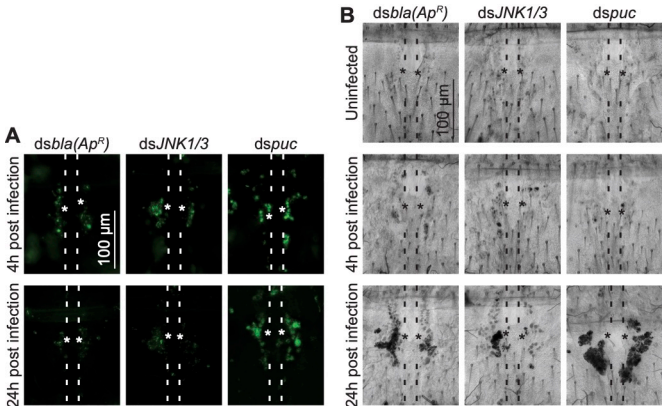

1091
1092
1093 **Figure 4–figure supplement 2. The JNK pathway affects GFP-*E. coli* and melanin**
1094 **accumulation at periostial regions.** (*A*) Fluorescence images show the accumulation
1095 of GFP-*E. coli* (green) around a single pair of ostia (asterisks) on a segment of the heart
1096 (outlined by dotted lines) of ds*bla(Ap^R)*, ds*JNK1/3* and ds*puc* mosquitoes that had been
1097 infected with GFP-*E. coli* for 4 or 24 hr. (*B*) Bright field images show the accumulation of
1098 melanin (dark deposits) around a single pair of ostia (asterisks) on a segment of the
1099 heart (outlined by dotted lines) of ds*bla(Ap^R)*, ds*JNK1/3* and ds*puc* mosquitoes that
1100 were not infected or had been infected with GFP-*E. coli* for 4 or 24 hr. Anterior is on top.
1101 Quantification of all mosquitoes assayed is presented in figures 4D and 4E.
1102
1103